Electronic Supplementary Information

Temperature dependent photoluminescence down to 77 K of organotin molecular rotors: Eco-friendly synthesis, photophysical characterization, X-ray structures, and DFT studies.

Arelly M. Cantón-Díaz,[a] Blanca M. Muñoz-Flores,[a] Luis F. Macías-Gamboa,[a] Ivana Moggio,[b] Eduardo Arias,[b] Gleb Turlakov,[b] H. V. Rasika Dias,[c] Gioele Colombo,[d] Stefano Brenna,[d] and Víctor M. Jiménez-Pérez.[a,*]

Content

Table S1. Crystal data of compounds **6** and **8**.	7
Fig. S1. ^{1}H NMR (DMSO-d_6) spectrum of terephthalic acid from PET waste.	13
Fig. S2. ^{13}C NMR (DMSO-d_6) spectrum of terephthalic acid from PET waste.	13
Fig. S3. ^{1}H NMR ($CDCl_3$) spectrum of **1**.	14
Fig. S4. ^{1}H NMR ($CDCl_3$) spectrum of **1** from PET waste.	14
Fig. S5. ^{1}H NMR ($CDCl_3$) spectrum of **3**.	15
Fig. S6. ^{1}H NMR (DMSO-d_6) spectrum of **3** from PET waste.	15
Fig. S7. ^{13}C NMR (DMSO-d_6) spectrum of **3** from PET waste.	16
Fig. S8. High resolution mass spectrum of **3**.	16
Fig. S9. Elemental composition calculator of **3** $C_8H_{11}N_4O_2$.	17
Fig. S10. ^{1}H NMR ($CDCl_3$) spectrum of ligand **4**.	17
Fig. S11. ^{1}H NMR ($CDCl_3$) spectrum of compound **5**.	18
Fig. S12. COSY ($CDCl_3$) spectrum of organotin compound **5**.	18
Fig. S13. ^{13}C NMR ($CDCl_3$) spectrum of compound **5**.	19
Fig. S14. HETCOR ($CDCl_3$) spectrum of organotin compound **5**.	19
Fig. S15. ^{119}Sn NMR ($CDCl_3$) spectrum of compound **5**.	20
Fig. S16. ^{1}H NMR ($CDCl_3$) spectrum of compound **6**.	20
Fig. S17. COSY ($CDCl_3$) spectrum of organotin compound **6**.	21
Fig. S18. ^{13}C NMR ($CDCl_3$) spectrum of compound **6.**	21
Fig. S19. HETCOR ($CDCl_3$) spectrum of organotin compound **6**.	22
Fig. S20. ^{119}Sn NMR ($CDCl_3$) spectrum of compound **6**.	22
Fig. S21. Infrared spectrum of terephthalic acid obtained from PET waste.	23
Fig. S22. Infrared spectrum of **1** obtained from PET waste.	23
Fig. S23. Infrared spectrum of **3** obtained from PET waste.	23
Fig. S24. Infrared spectrum of compound **4**.	24
Fig. S25. Infrared spectrum of compound **5**.	24
Fig. S26. Infrared spectrum of compound **6**.	24

Fig. S27. High resolution mass spectrum of compound **4**.	25
Fig. S28. High resolution mass spectrum of compound **5**.	25
Fig. S29. Isotopic pattern of compound **5**.	26
Fig. S30. High resolution mass spectrum of compound **6**.	26
Fig. S31. Thermogravimetric Analysis of compound **5**.	27
Fig. S32. Thermogravimetric Analysis of compound **6**.	27
Table S2. Calculated wavelength (λ) and oscillator strength (f, approximated to the first two digits) for the 30 excitations of complex **5** and **6**.	28
Table S3. Fluorescence lifetimes in chloroform at different excitation and fluorescence emission value.	30
Fig. S33. Fluorescence spectra of organotin compound **5** in $CHCl_3$ at different excitation wavelength. Inserted figure: corresponding excitation spectrum by fixing as emission value: 496, 533 or 580 nm.	31
Fig. S34. TCSPC Fluorescence decay (symbols) and fit (dotted lines) of organotin compound **5** (left graphs) and **6** (right graphs) in $CHCl_3$ at 370 nm (top panel) or 455 nm (bottom panel) excitation. The emission wavelengths are specified in the legend..	32
Fig. S35. Fluorescence spectra of organotin compound **6** in chloroform at different temperatures.	33
Fig. S36. Fluorescence spectra of ligand **4** in 2-methyl tetrahydrofuran ($5 \cdot 10^{-5}$ M) at different temperatures.	33
Fig. S37. Fluorescence spectra of organotin compound **5** in 2-methyl tetrahydrofuran ($5 \cdot 10^{-5}$ M) at different temperatures.	34
Fig. S38. Fluorescence spectra of organotin compound **6** in 2-methyl tetrahydrofuran ($5 \cdot 10^{-5}$ M) at different temperatures.	34
Table S4. Average weighted fluorescence lifetimes of complex **5**, at different temperatures, recorded in 2-methyl tetrahydrofuran ($5 \cdot 10^{-5}$ M).	35
Table S5. Fluorescence lifetimes of compound **4**, at different temperatures, recorded in 2-methyl tetrahydrofuran ($5 \cdot 10^{-5}$ M).	36
Fig. S39. Tapping AFM image of thin film prepared from chlorobenzene solutions of complex **5** in 25 μm*25 μm scanning area and (inset) 5 μm*5μm.	37
Fig. S40. Molecular structure of compound **8**.	38
Fig. S41. Current profiles of Sn-complex **5** at different orientations as signaled in the STM image: for the lamellae length determination and right) for the individual molecules length determination: Vbias = -740 mV, It = 90 pA.	39
Fig. S42. Topographic profiles of Sn-complex **6** at different orientations as signaled in the STM image: left) for the lamellae length determination and right for the individual molecule's length determination: Vbias = -830 mV, It = 110 pA.	40

Fig S43. (a) Successive cyclic voltammogram of binuclear Sn-complex **5** in CH_2Cl_2 (0.1 mmol), at scan rate of 50mV/s vs. Ag/AgCl, using GC as working electrode and 0.1 M Bu_4NPF_6 as supporting electrolyte. (b) Cyclic voltammograms of the (left) reductive (0 to +3 V) and (right) oxidative (0 to -2.40 V). By analysing the redox process by separate, this is not completely carried out (as occurs with the complete cycle), suggesting that in order to reduce **5**, it needs to be oxidized and vice versa; the anions or cations can be individually stabilized once formed within the structure.	41
Fig S44. (a) Successive cyclic voltammogram of binuclear Sn-complex **6** in CH_2Cl_2 (0.1 mmol), at scan rate of 50mV/s vs. Ag/AgCl, using GC as working electrode and 0.1 M Bu_4NPF_6 as supporting electrolyte. (b) Cyclic voltammograms of the (left) reductive (0 to +3 V) and (right) oxidative (0 to -2.40 V). By analysing the redox process by separate, this is not completely carried out (as occurs with the complete cycle), suggesting that in order to reduce **6**, it needs to be oxidized and vice versa; the anions or cations can be individually stabilized once formed within the structure.	41
References	42

1. **General considerations**

1.1. Materials and measurements

All starting materials such Bu_2SnO, Ph_2SnO, dimethylterephthalate, hydrazine monohydrate and organic solvent were purchased from Aldrich Chemical Company. 2-Methyltetrahydrofuran (stabilized with BHT) was purchased from TCI chemicals. Solvents were used without further purification. The synthesis of all complexes was performed with Anton Paar Monowave 300 microwave reactor. Melting points were carried out on an Electrothermal Mel-Temp apparatus and are uncorrected. Infrared spectra were recorded using a Bruker Tensor 27 FT-IR spectrophotometer equipped with a Pike Miracle™ ATR accessory with single reflection ZnSe ATR crystal. Raman spectra were obtained with a Horiba Xplora equipment, focusing the sample as powders on a microscopic slide with a 10X objective. The excitation wavelength was 785 nm and the Nanoled power was 10% of total laser power (25 mW). Spectra were acquired with 10s acquisition time and 10 accumulations, spectral resolution of 2 cm^{-1}. High-resolution mass spectra were acquired by LC/MSD TOF on an Agilent Technologies instrument with APCI as ionization source. ^{1}H, ^{13}C and ^{119}Sn-NMR spectra were recorded in $CDCl_3$ and $(CD_3)_2SO$ on a Bruker advance DPX 400. Chemical shifts (ppm) are relative to $(CH_3)_4Si$ for ^{1}H and ^{13}C and to $(CH_3)_4Sn$ for ^{119}Sn. The

thermal stability of compounds (vacuum dried samples) was determined in a thermogravimetric analyser (TGA 951 from DuPont Instruments) connected to a N_2 vector gas, heating from 25 to 600 °C at 10 °C min^{-1}.

1.2. Theoretical calculations

All theoretical calculations were performed with Orca, version 5.0.1.[1] Geometry optimizations in chloroform via LR-CPCM[2] in equilibrium conditions were performed with the B3LYP functional, including D3BJ dispersion correction with Becke–Johnson damping[3] and considering scalar relativistic the zeroth-order regular approximation (ZORA).[4] For light elements, H, C, O and N Hamiltonian-specific recontractions of all-electron nonrelativistic Karlsruhe basis sets[5] were used, while for Sn specially designed segmented all-electron relativistically contracted (SARC) basis set[6] was employed for both geometry optimization and TDDFT calculations in combination with corresponding auxiliary SARC/J and def2-TZVP/C basis sets. Analytical frequencies were computed for all optimized structures and the absence of imaginary modes confirmed that true minima were obtained in all cases. The excited states analysis was performed using Multiwfn 3.8.[7] Electrostatic potential maps (MEP) were plotted for the optimized geometries using VMD program.[8] The blue colour represents positive electrostatic potential while the red one corresponds to negative electrostatic potential and the green is attributed to zero potential. All calculations were made on cluster Thubat Kaal II of National Supercomputing Center-IPICYT.

1.3. Photophysical characterization

For the determination of the intrinsic photophysical properties, dilute solutions (~10^{-6}M) in freshly distilled spectroscopic grade $CHCl_3$ (Sigma-Aldrich) were studied as prepared, to avoid any solvolysis or photodegradation effect.[9] The UV-Vis absorption spectra were recorded on a Shimadzu 2401PC spectrophotometer. The extinction coefficient was obtained from the slope of the absorbance vs. molar concentration for four solutions. Optical band gap (*Eg*) corresponds to the value where the X axis (energy) crosses the tangent drawn at absorbance of 0.1 of the normalized absorption spectra. The excitation and emission spectra were obtained with a Horiba PTI Quantamaster QM-8450-22-c spectrofluorimeter, equipped with an integrating sphere for the determination of the quantum yield and a Peltier accessory for the temperature studies (with refrigerator liquid for a temperature range between -10 to

40 °C). All the spectra were obtained with background correction. The excitation wavelength was 10 nm below the main absorption peak and the absorbance at that wavelength was adjusted to be lower than 0.1. Three solutions were analysed for each complex and the quantum yield was averaged. Stokes' shift values were calculated from the absorption and fluorescence maximums. Fluorescence lifetimes were obtained at room temperature by the time correlated single photon counting (TCSPC) technique by using the kinetic module of the same spectrofluorimeter with a nanoLED laser (1.2 ns of pulse, 370 nm or 455 nm). Fits were performed with the Felix software of the instrument. Aggregation studies were carried out in THF/water mixtures increasing the water content from 0 to 90% with a 10% volume percent increase.)

The emission spectra at lower (25 to -196 °C) in 2-methyl tetrahydrofuran (Me-THF) were collected on a Photon Technology International (PTI) QuantaMaster QM-40 spectrometer equipped with a Xe arc lamp (70 W), utilizing a quartz cold finger Dewar accessory. The corresponding lifetimes measurements were performed on an Edinburgh Instruments FS5 fluorimeter equipped with an EPLED-320 (Edinburgh Instruments) as the pulsed source. Analysis of the lifetime decay curve was done using Fluoracle® Software package (Ver. 1.9.1) which runs the FS5 instrument.

Fluorescence quantum yields at low temperatures in 2-methyl tetrahydrofuran were estimated indirectly using the following equation:

$$\Phi_T = \Phi_{RT}\frac{I_T}{I_{RT}} \qquad \text{(Eq. 1)}$$

where Φ_T is the fluorescence quantum yield calculated at a given temperature, Φ_{RT} is the fluorescence quantum yield obtained experimentally at room temperature, I_T is the maximum intensity of the emission spectrum at a given temperature and I_{RT} is the maximum intensity of the emission spectrum recorded at room temperature. The correction depending on the refractive index has been neglected due to lack of experimental data regarding the refractive indexes of 2-methyl tetrahydrofuran at all the temperatures; for this reason, the calculated fluorescence quantum yields have to be intended as estimates and not as absolute values.

For the films characterization, samples were prepared on quartz slides (Spi.Inc) by spin coating with a WS-400B-6NPP-LITE spin processor from Laurell Technologies. A 30 mg/mL C_6H_5Cl solution was spun with a first step of 25s at 1000 rpm speed and a second step of 20s at 2500 rpm. These parameters were optimized after different assays to have a good homogeneity and thickness around 100 nm as found by AFM, using a Veeco Digital Instruments 3100 microscope in tapping mode at a scanning rate of 0.2 Hz. UV-Vis powder spectra were recorded in diffuse reflectance mode, with the same spectrophotometer used for the solutions, coupled with an integrating sphere.

1.4. X-ray crystallography

The crystal of **6** was covered with a layer of hydrocarbon oil that was selected and mounted with paratone-N oil on a cryo-loop, and immediately placed in the low-temperature nitrogen stream at 100(2) K (Table 1). The data for **6** was recorded on a Bruker SMART APEX CCD area detector system equipped with an Oxford Cryosystems 700 Series Cryostream cooler, a graphite monochromator, and a Mo Kα fine-focus sealed tube (λ = 0.71073 Å). The structure was solved by direct methods using SHELXS-97[10] and refined against F^2 on all data by full-matrix least-squares with SHELXL-97.[11] All of the software manipulations were done under the WIN-GX environment program set.[12] All the heavier atoms were found by Fourier map difference and refined anisotropically. Some hydrogen atoms were found by Fourier map differences and refined isotropically. The remaining hydrogen atoms were geometrically modelled and were not refined. The measurements for XRD the samples were made in a range of 2θ 0-90◦ with a step size of 0.01◦ and a counting time of 4.5 s for step. The CCDC numbers are 1871586 and 2293069 for **6** and **8**, respectively.

Table S1. Crystal data of compounds **6** and **8**.

	6	**8**
Empirical formula	$C_{54}H_{38}N_4O_4Sn_2$	$C_{32}H_{24}N_2O_4Sn$
Formula weight	1044.26	619.2
Temperature, K	100(2)	298(2)
Wavelength Å	0.71073	0.71073
Crystal system	Triclinic	Monoclinic
Space group	*P*-1	*P*2(1)/*c*
a, Å	9.1150(8)	14.1091(10)
b, Å	10.5354(9)	21.6813(14)
c, Å	12.3958(11)	9.2066(6)
α	80.286(2)°	90.00°
β	72.486(2)°	101.065(2)°
γ	68.711(2)°	90.00°
V,Å^3	1055.35(16)	2764.0(3)
Z	1	2
$\rho_{calc,mg.cm^{-3}}$	1.643	1.488
μ, mm^{-1}	1.239	0.963
F(000)	522.0	1248.0
Crystal size/mm^3	0.15 x 0.14 x 0.06	0.35 x 0.28 x 0.1
Radiation	MoKα (λ = 0.71073)	MoKα (λ = 0.71073)
2θ range for data collection	6.752 to 61.018°	2.386–29.209°
Index ranges	-12 ≤ *h* ≤ 13, -15 ≤ *k* ≤ 15, -17 ≤ *l* ≤ 17	-19 ≤ *h* ≤ 19, -29 ≤ *k* ≤ 29, -12 ≤ *l* ≤ 12
No. of reflns collected	14656	157026
No. of indep reflns	6385	5649
[R_{int}]	0.0185	0 .0443
Goodness of fit	1.057	1.108
*R*1, w*R*2 (I>2σ(I))	0.0216/0.0540	0.0353/0.0826
*R*1, w*R*2 (all data)	0.0239/0.0550	0.0453/0.0885
Largest diff. peak/hole/ e Å^{-3}	0.69/-0.75	0.80/-0.68
CCDC number	1871586	2293069

1.5. Electrochemistry

Cyclic voltammetry was performed in a C3 Stand cell from Basi, coupled to an ACM Gill AC potentiostat/galvanostat. The system consisted in a conventional three-electrode cell: glacy carbon as a working electrode (polished with alumina after each run), Pt wire as the counter electrode, Ag/AgCl as reference electrode and ferrocene/ferrocenium as internal reference (at the maximum potential: E_{ox}= 0.590 V, E_{red}= 0.510 V); a value of -4.8 eV below the vacuum level was considered. Voltammetric measurements were performed at room temperature in acetonitrile containing Bu_4NPF_6 (0.1M) as the supporting electrolyte. Prior to recording the voltammograms, all the solutions (~0.1 mmol) were deoxygenated by bubbling nitrogen at least for 15 min. The experiments were carried out under nitrogen atmosphere at a scanning rate of 50 mV/s.

1.6. STM characterization.

It was performed between ~23 and 25° C using an AA5000 Scanning Probe Microscope (Angstrom Advanced Inc., Braintree, MA USA). The scanner tube calibration was performed by means of atomic resolution images obtained using commercial HOPG substrates from Ted Pella (Redding, CA USA) and SPI Supplies (grade SPI-3). Samples were exfoliated before each measurement by the adhesive tape method. Pt/Ir tips were prepared by mechanically cutting a 0.25 mm diameter 80/20 wire from Nanoscience, Switzerland. 1,2,4-tricholorobenzene (TCB) (Sigma Aldrich, ≥ 99 %) was used as received. The Sn-complexes **5**, **6** were dissolved in TCB (2.8 mM), sonicated and heated to 60 °C for one hour. A droplet of the solution, ~3 µL, was placed by using a micro-syringe between the substrate and tip, then a pulse of 2 - 6 V was applied up to obtain a monolayer. STM images were taken in the constant-current mode at the solid-liquid interface. The bias and current values were constantly adjusted during each scan. Details on the experiment bias and current set-point are given below each image. The raw and FFT images were processed from WSxM 5.0 software with the aim to reduce noise and normally observed drift.[13]

1.7. The general procedure of synthesis of precursor

1.7.1. Synthesis of terephthalate acid from PET waste.

Sodium hydroxide (200 mg) was dissolved in 10 ml ethanol and PET waste (500 mg) was added. The reaction mixture was synthesized by irradiation of microwave for 30 min. The product precipitate from the mixture. After cooling to room temperature, the precipitate was filtered, washed with ethanol thoroughly and dried completely to give solid white powder. Then, the product was dissolved in water and 4-5 drops of conc. HCl was added to precipitate the terephthalate acid, the precipitate was filtered, washed with ethanol thoroughly and dried complete to give solid white powder. Yield 417 mg (96%). m. p. 300 °C. $IR_{\upsilon max}$ (ATR): 3063 (C-H, ArH), 2817 (OH), 1678 (C=O), 728 (C-H ArH). UV/vis (DMSO) λ_{abs} (nm): 287 [0.44]. Fluorescence (DMSO): λ_{em} (nm): 363. ^{1}H NMR (400 MHz, DMSO-d_6, 298 K): δ = 8.06 (s, 4H, ArH), 13.30 (s, 2H, OH) ppm. ^{13}C NMR (100.61 MHz, DMSO-d_6, 298 K): δ = 129.6 (C3), 134.6 (C2), 166.8 (C1) ppm.

*1.7.2. Synthesis of diethyl terephthalate (**1**) rute 1*

Terephthalic acid (1.6 g) in ethanol dry (60 mL) containing 2-3 drops of conc. H_2SO_4 (AR) was refluxed till it dissolves. Then, the reaction mixture was poured on to ice cold water, immediately a solid started separating from the clear solution. Then sodium bicarbonate was used to neutralize the acid excess. The ester was filtered, washed several times with water, and dried in air. Yield: 84% (1.79 g). m. p. 44 °C (Lit.[14] m. p. 44.5 °C). ^{1}H NMR (400.13 MHz, $CDCl_3$, 298 K): δ = 1.42 (t, J = 7.0 Hz, 6H; CH_3), 4.40 (q, J = 7.7 Hz, 4H; CH_2), 8.10 (s, 4H, aryl) ppm.

*1.7.3. Synthesis of diethyl terephthalate (**1**) rute 2 from PET waste.*

PET waste (500 mg) was added in 10 ml ethanol containing conc. H_2SO_4 (2 mL). The reaction mixture was synthesized by irradiation of microwave for 60 min. The product precipitated from the mixture. After cooling to room temperature, the precipitate was filtered, washed with ethanol thoroughly and dried completely to give solid white powder. Yield 262 mg (82%). m. p. 45 °C. $IR_{\upsilon max}$ (ATR): 2968 (C-H, ArH), 1717 (C=O), 1250 (C-O), 725 (C-H ArH). UV/vis ($CHCl_3$) λ_{abs} (nm): 299 [0.07]. Fluorescence ($CHCl_3$): λ_{em} (nm): 347. ^{1}H

NMR (400.13 MHz, $CDCl_3$, 298 K): δ = 8.10 (s, 4H, ArH), 4.69 (q, 4H, CH_2), 0.07 (t, 6H, CH_3) ppm. ^{13}C NMR (100.61 MHz, $CDCl_3$, 298 K): δ = 129.6 (C3), 134.6 (C2), 166.8 (C1) ppm.

*1.7.4. Synthesis of dihydrazide (**3**) rute 1.*

A mixture of diethyl terephthalate 0.5 g (2.25 mmol) was dissolved in 50 mL ethanol and hydrazine monohydrate (1 ml) was added. The reaction mixture was refluxed for 24 h. The product precipitated from the mixture. After cooling to room temperature, the precipitate was filtered, washed with water thoroughly and dried completely to give solid white powder. Yield 4.27 g (81 %). m.p. >300 °C (Lit.[15] m. p. >300 °C). ^1H NMR (400 MHz, DMSO-d_6, 298 K): δ= 9.89 (s, 2H), 7.87 (s, 4H), 4.59 (s, 4H J = 5.0 Hz) ppm.

*1.7.5. Synthesis of dihydrazide (**3**) rute 2*

Preparation of route 2 was accomplished following the same procedure of route 1 with 50 ml methanol. Yield 4.27 g (81 %). m. p. >300 °C. ^1H NMR (400 MHz, DMSO-d_6, 298 K): δ= 9.89 (s, 2H), 7.87 (s, 4H), 4.59 (s, 4H J=5.0 Hz). (Lit.[16] m. p. >300 °C)

*1.7.6. Synthesis of dihydrazide (**3**) rute 3*

A mixture of dimethyl terephthalate 0.2 g (1.03mmol) was dissolved in 5 ml methanol and hydrazine monohydrate (0.45 ml) was added. The reaction mixture was synthesized by irradiation of microwave for 20 min. The product precipitated from the mixture. After cooling to room temperature, the precipitate was filtered, washed with water and methanol thoroughly and dried completely to give solid white powder. Yield 0.19 g (95%). m. p. >300 °C. ^1H NMR (400 MHz, DMSO-d_6, 298 K): δ= 9.87 (s, 2H), 7.86 (s, 4H), 4.54 (s, 4H) ppm.

*1.7.7. Synthesis of dihydrazide (**3**) rute 4 from PET waste.*

PET waste (500 mg) was added in 10 ml ethanol and hydrazine monohydrate (1.25 mL) was added. The reaction mixture was synthesized by irradiation of microwave for 60 min. The product precipitated from the mixture. After cooling to room temperature, the precipitate was filtered, washed with ethanol thoroughly and dried completely to give a solid white powder. Yield 409 mg (81%). m. p. 370 °C. $IR_{\upsilon max}$ (ATR): 3313 (NH), 3029 (C-H, ArH), 1602 (C=O), 1100 (C-N), 736 (C-H ArH). UV/vis (DMSO) λ_{abs} (nm) [ε_{max} *10^4 (M^{-1} cm^{-1})]: 312 [0.21]. Fluorescence (DMSO): λ_{em} (nm): 383. ^1H NMR (400 MHz, DMSO-d_6,

298 K): δ = 4.57 (s, 4H, NH_2), 7.86 (s, 4H, ArH), 9.89 (s, 2H, NH) ppm. ^{13}C NMR (100.61 MHz, DMSO-d_6, 298 K): δ = 127.0 (C3), 135.5 (C2), 165.2 (C1) ppm. HRMS (TOF) $C_8H_{11}N_4O_2$. [M+] Found: 195.087652, ppm error: -0.892786.

*1.8. The general procedure of synthesis of ligand and organotin compounds **1-2** and Schiff base.*

*1.8.1. Bis(2-hydroxy-1-naphthaldehyde)terephthalohydrazone(**4**)*

A mixture of terephthalohydrazide 0.10 g (0.51 mmol) and 2-hydroxy-1-naphthaldehyde 0.20 g (0.10 mmol) was refluxed in methanol for 24 hr. The yellow solid formed was filtered, washed with methanol and vacuum dry. Yield 0.17 g (68 %). m. p. 345° C. $IR_{\upsilon max}$ (ATR): 3189 (s, N-H), 3003 (s, O-H), 1640 (s, C=O), 1622 (m, C=N). ^1H NMR (400 MHz, DMSO-d_6, 298 K): δ = 12.84 (s, 2H, OH), 12.29 (s, 2H, NH), 9.57 (s, 2H, CH), 8.20 (d, J = 8.0 Hz, 2H, Np), 7.59(t, J = 7.6 Hz, 2H, Np), 7.40 (t, J = 7.6 Hz, 2H, Np) 7.21 (d, J = 8.8 Hz, 2H, Np) ppm. HRMS (APCI/TOF-Q) *m/z*: 484.1503 [M+] Found: 502.1641 PPM error: -0.1445

*1.8.2. Synthesis of Bis(2-hydroxy-1-naphthaldehyde)terephthalohydrazone di-n-butyltin(IV) (**5**)*

A microwave tube was placed with a magnetic shuffler, it was added terephthalohydrazide 0.05 g (0.25 mmol) and 2-hydroxy-1-naphthaldehyde 0.08 g (0.51 mmol) more dibutyltin oxide 0.12 g (0.51 mmol) in acetonitrile 5 mL were heated to 180°C for 20 min. After this time, the solution was cooled, and the solvent evaporated under reduced pressure and washed with hexane and acetonitrile. The precipitate was collected by filtration and crystalized with dichloromethane/methanol (1:1) to afforded 0.20 g (0.19 mmol, 76% yield) of **5** as orange-yellow solid. m. p. 172°C. $IR_{\upsilon max}$ (ATR): 3057 (C-H ArH), 2326 (O-C=N) 1602 (C=N), 1581 (C=N-N=C), 715 (C-H ArH). UV/vis ($CHCl_3$) λ_{abs} (nm) [ε_{max} *10^4 ($M^{-1}\,cm^{-1}$)]: 456 [0.08]. Fluorescence ($CHCl_3$): λ_{em} (nm): 495. ^1H NMR (400.13 MHz, $CDCl_3$, 298 K): δ = 9.73 [s, 2H, $^3J(^1H–^{119}Sn)$ = 45.08 Hz H-11], 8.14 (s, 4H, ArH, H-14), 8.09 - 8.11 (d, J = 12 Hz, 2H, H-9), 7.76-7.78 (d, J = 8 Hz, 2H, H-4), 7.69-7.71 (d, J = 8.0 Hz, 2H, H-6), 7.53 (t, J = 16 Hz, 2H, H-8), 7.33 (t, J = 8 Hz, 2H, H-7), 6.95-6.97 (d, J = 8.0 Hz, 2H, H-3), 1.40 (t, 6H, ^3J = 7.2 Hz, CH_3- γ), 0.85-0.89 (m, 4H, CH_2- δ), 1.55-1.59 (t, 4H, ^3J = 7.2

Hz, CH_2- α), 1.65-1.71 (m, 4H, ^3J = 7.2 Hz, CH_2- β). ^{13}C NMR (100.61 MHz, $CDCl_3$, 298 K): δ = 13.41 (δ, CH_3,), 26.27 [Cγ, $^3J(^{13}C\text{-}^{119}Sn)$ = 83.86 Hz], 26.66, [Cβ, $^2J(^{13}C\text{-}^{119}Sn)$ = 33.75 Hz], 21.87 [Cα, $^1J(^{13}C\text{-}^{119}Sn)$ = 595/568 Hz], 107.24 (C1), 169.24 (C2), 119.31 (C3), 136.81 (C4), 127.31 (C5), 128.18 (C6), 123.15 (C7), 124.52 (C8), 129.30 (C9), 135.97 (C10), 157.26 (C11), 168.17 (C12), 135.83 (C13), 127.51 (C14) ppm. ^{119}Sn NMR (128.0 MHz, C_6D_6, 298 K): δ = - 189.28 ppm. HRMS (APCI/TOF-Q) *m/z*: 966.2261 [M+] Found: 967.226181, ppm error: 0.1445.

*1.8.3. Synthesis of Bis(2-hydroxy-1-naphthaldehyde)terephthalohydrazone diphenyltin(IV) (**6**)*

Preparation of **6** was accomplished following the same procedure of **4** from terephthalohydrazide 0.05 g (0.25 mmol) and 2-Hydroxy-1-naphthaldehyde 0.08 g (0.51mmol) more diphenyltin oxide 0.14mg (0.51 mmol) to 180°C for 30 min. Yield: 0.23g (0.52 mmol, 75%). Yellow solid. m. p. 336°C. $IR_{\upsilon max}$ (ATR): 3065 (C-H ArH), 2326 (O-C=N), 1580 (C-N-N-C), 1596 (C=N), 1582 (C=N-N=C), 715 (C-H ArH). UV/vis ($CHCl_3$) λ_{abs} (nm) [ε_{max} *10^4 (M^{-1} cm^{-1})]: 453 [0.07]. Fluorescence ($CHCl_3$): λ_{em} (nm): 491. ^{1}H NMR (400 MHz, $CDCl_3$, 298 K): δ = (9.78 [s, 2H, $^3J(^1H\text{–}^{119}Sn)$ = 56 Hz H-11], 8.39 (s, 4H, ArH, H-14), 8.09-8.12 (d, *J* = 12 Hz, 2H, H-9), 7.91-7.93 (d, *J* = 8 Hz, 2H, H-4), 7.73-7.78 (d, *J* = 8.0 Hz, 2H, H-6), 7.54 (t, *J* = 16 Hz, 2H, H-8), 7.46 (t, *J* = 8Hz 2H, H-7), 7.42-7.43 (d, ^3J = 8.0 Hz, 2H, H-3), 7.91 (s, 8H, ^3J = 7.2 Hz, H-o), 7.43 (s, 8H, ^3J = 8.0 Hz, H-m), 7.45 (s, 4H, ^3J = 8.0 Hz, H-p). ^{13}C NMR (100.61 MHz, $CDCl_3$, 298 K): δ = 136.39 (H-o), 129.15 (H-m), 130.76 (H-p), 137.40 (C-i) 107.58 (C1), 169.78 (C2), 119.60 (C3), 141.43 (C4), 127.62 (C5), 129.35 (C6), 123.55 (C7), 124.64 (C8), 129.54 (C9), 134.00 (C10), 157.88 (C11), 167.72 (C12), 139.13 (C13), 127.51 (C14). ^{119}Sn NMR (100.7 MHz, C_6D_6, 298 K): δ = - 328.69 ppm. HRMS (APCI/TOF-Q) *m/z*: Calcd. For $C_{37}H_{37}NO_2Sn$ [M^+] 1046.0900 Found: 1047.1009 u.m.a. (Error: -0.8524 ppm)

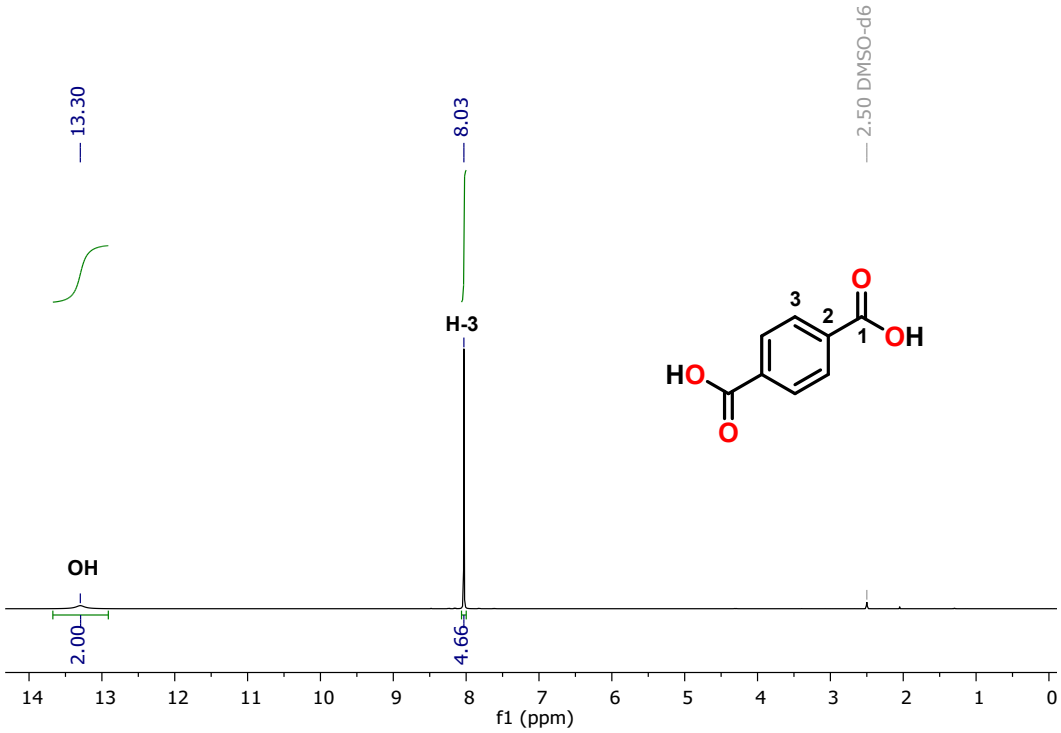

Fig. S1. ^{1}H NMR (400 MHz, DMSO-d_6) spectrum of terephthalic acid from PET waste.

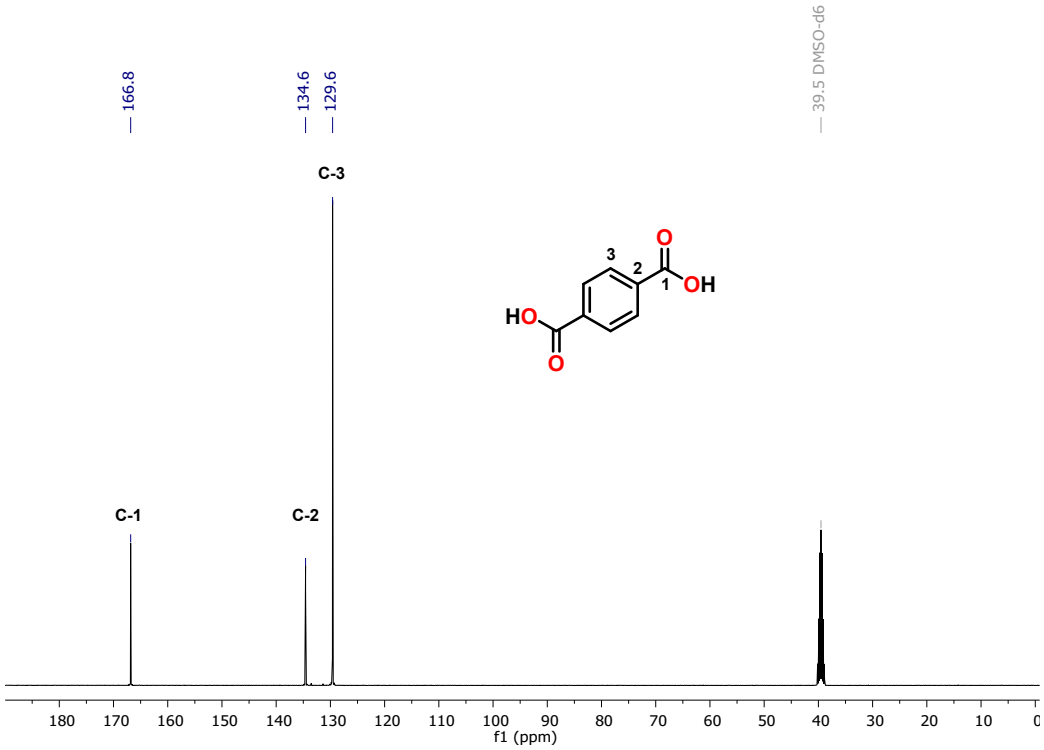

Fig. S2. ^{13}C NMR (100 MHz, DMSO-d_6) spectrum of terephthalic acid from PET waste.

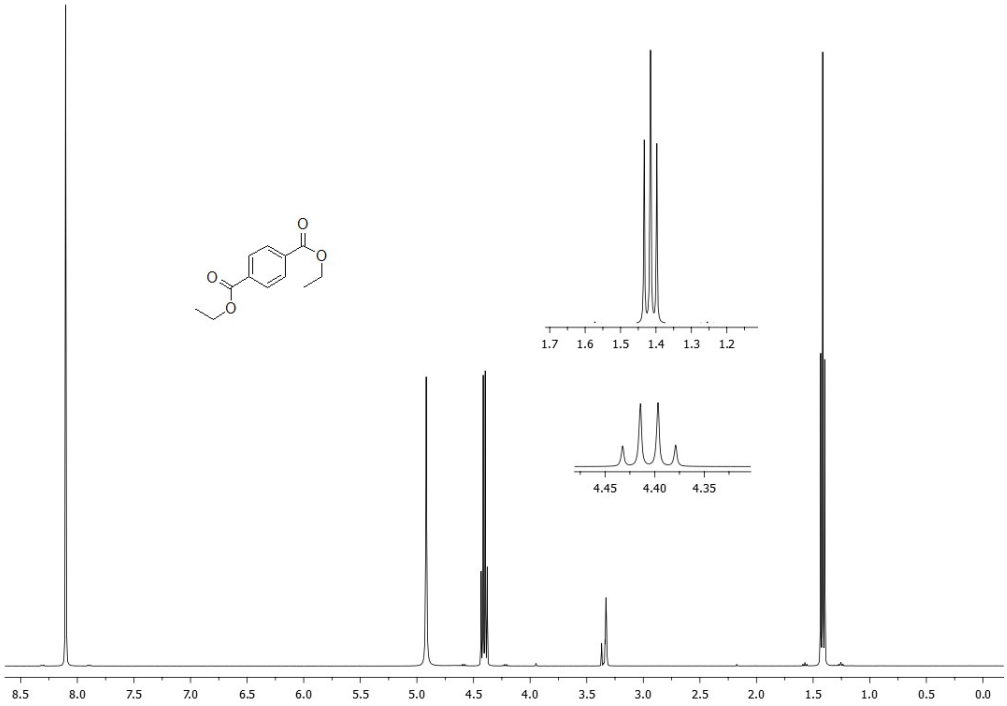

Fig. S3. ^{1}H NMR (400 MHZ, $CDCl_3$) spectrum of **1**.

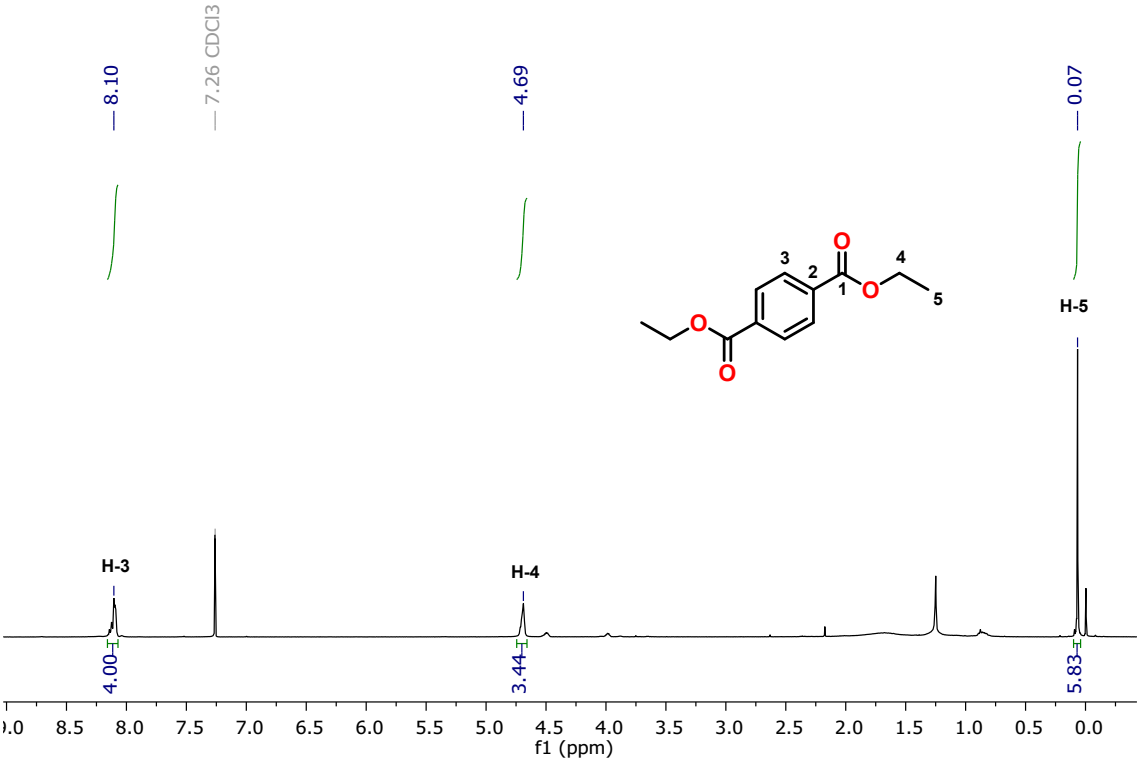

Fig. S4. ^{1}H NMR (400 MHz, $CDCl_3$) spectrum of **1** from PET waste.

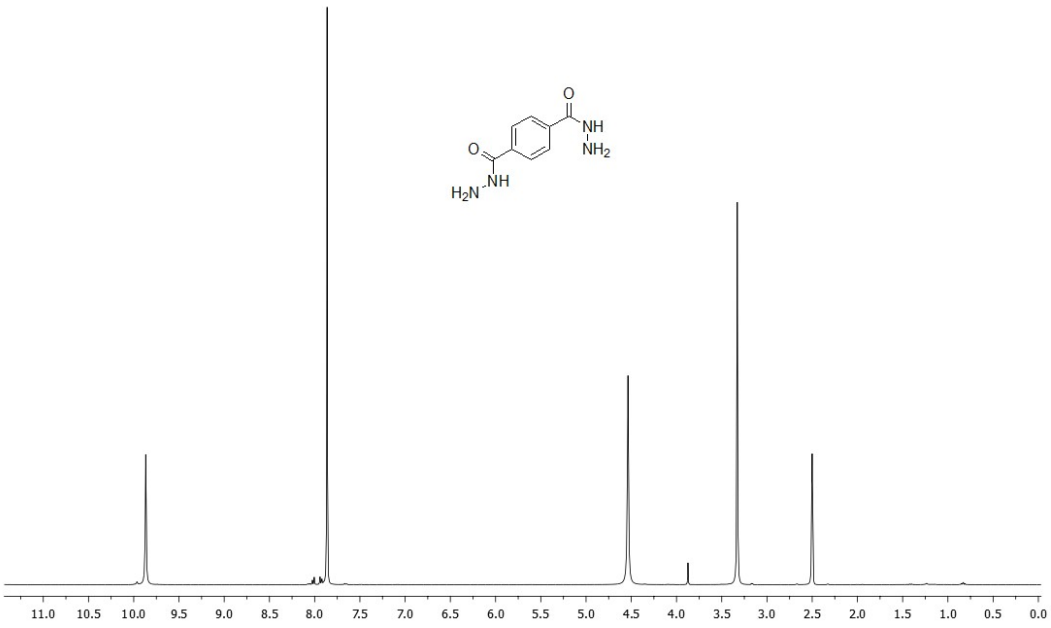

Fig. S5. ^{1}H NMR (400 MHz, $CDCl_3$) spectrum of **3**.

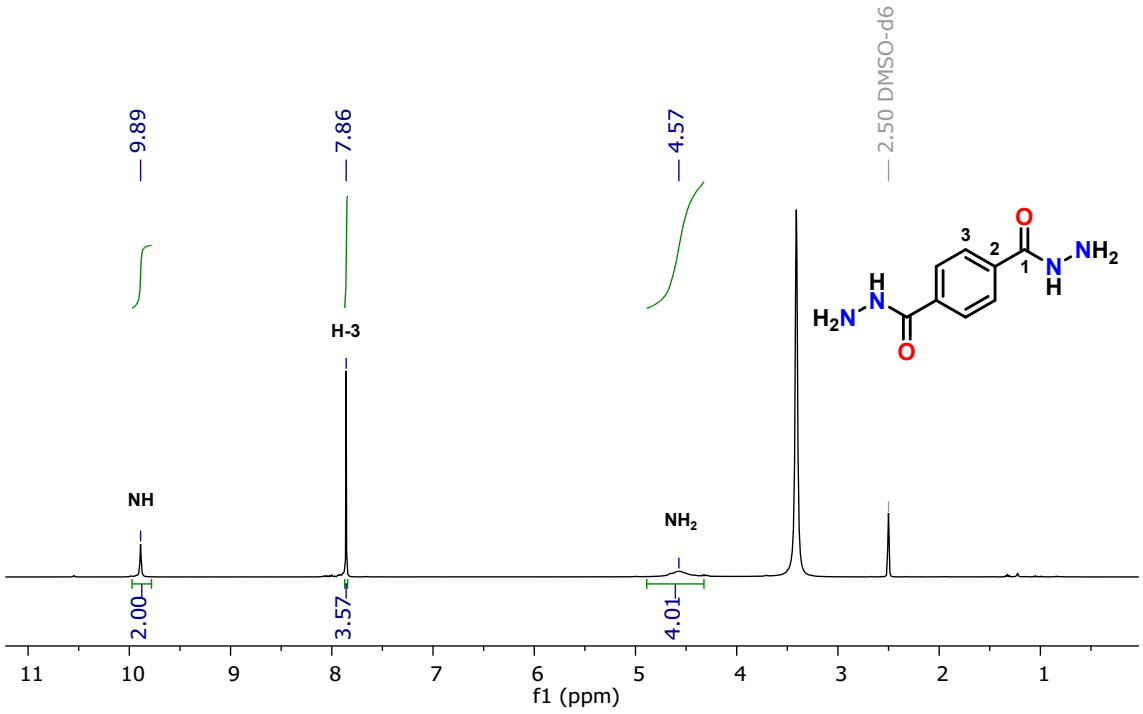

Fig. S6. ^{1}H NMR (400 MHz, DMSO-d_6) spectrum of **3** from PET waste.

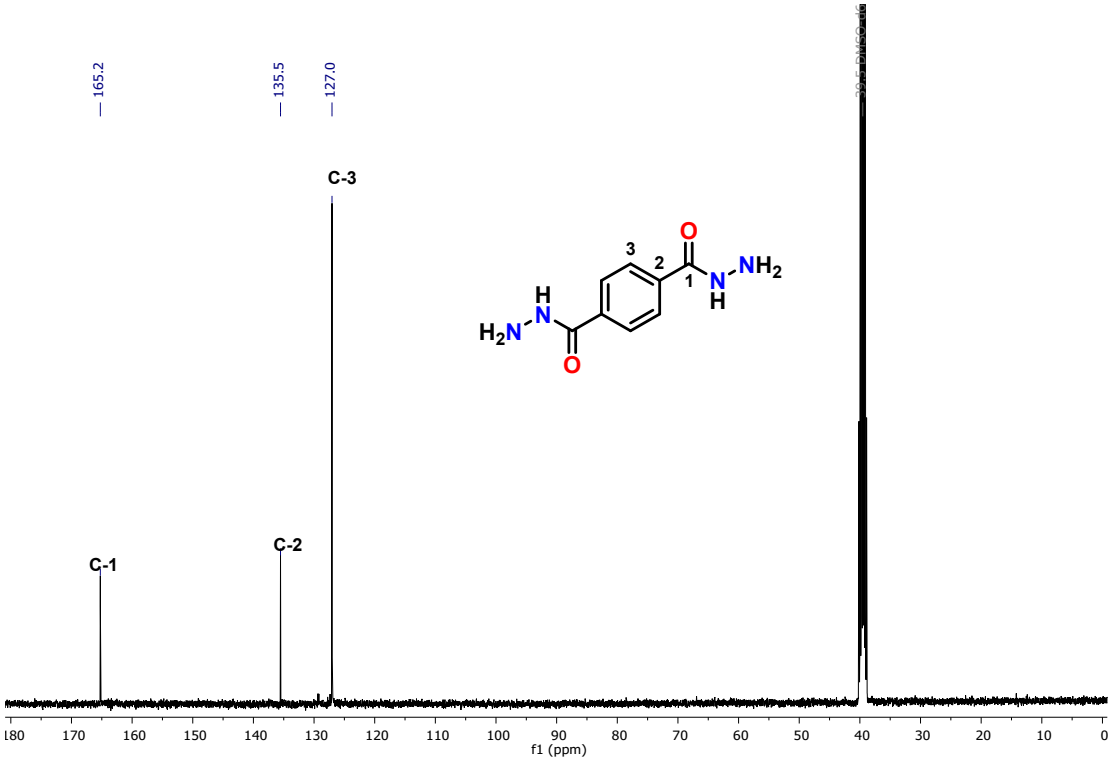

Fig. S7. ^{13}C NMR (100 MHz, DMSO-d_6) spectrum of **3** from PET waste.

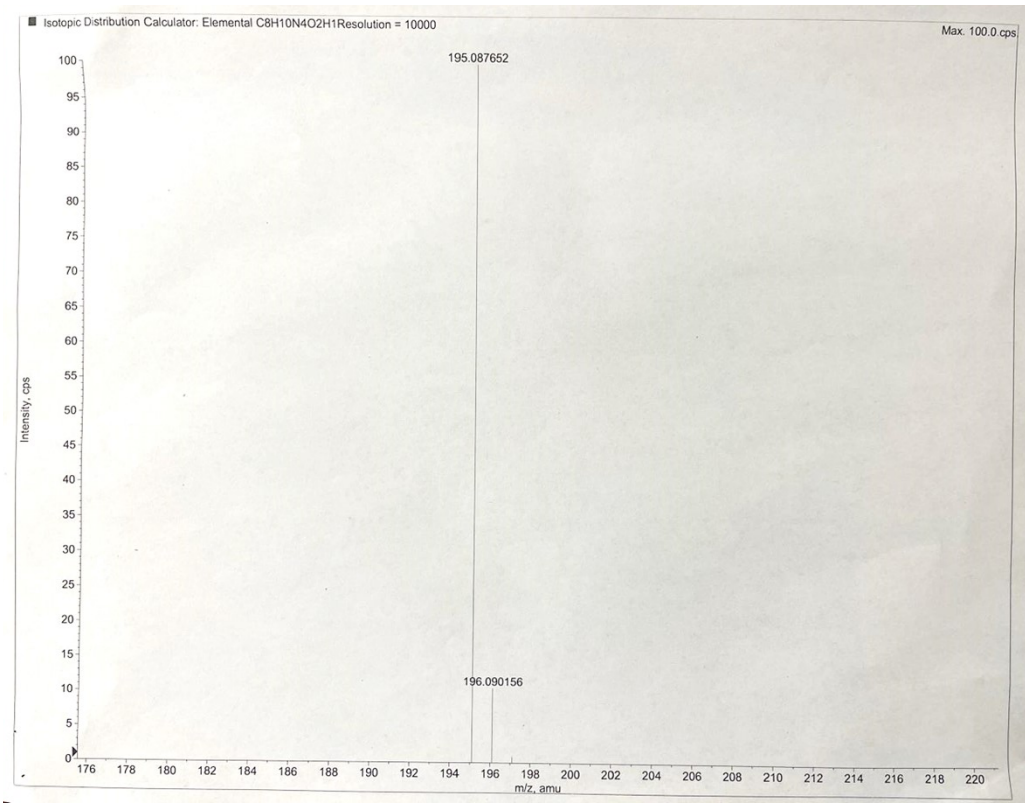

Fig. S8. High resolution mass spectrum of **3**.

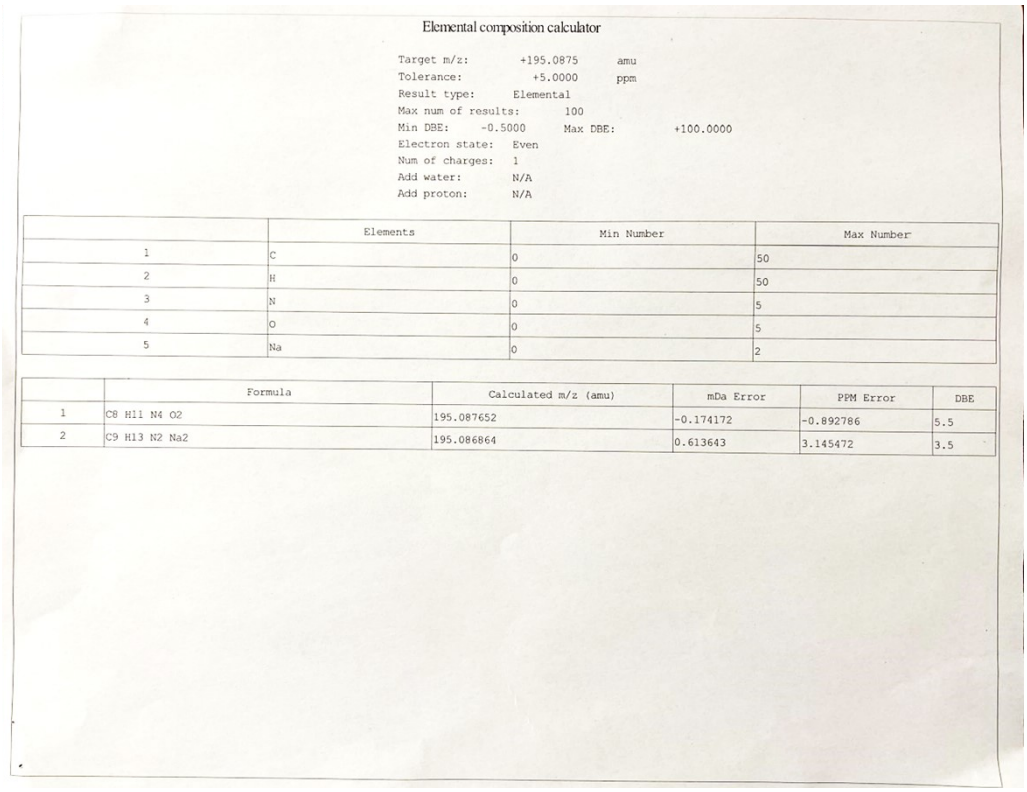

Elemental composition calculator

Target m/z: +195.0875 amu
Tolerance: +5.0000 ppm
Result type: Elemental
Max num of results: 100
Min DBE: -0.5000 Max DBE: +100.0000
Electron state: Even
Num of charges: 1
Add water: N/A
Add proton: N/A

	Elements	Min Number	Max Number
1	C	0	50
2	H	0	50
3	N	0	5
4	O	0	5
5	Na	0	2

	Formula	Calculated m/z (amu)	mDa Error	PPM Error	DBE
1	C8 H11 N4 O2	195.087652	-0.174172	-0.892786	5.5
2	C9 H13 N2 Na2	195.086864	0.613643	3.145472	3.5

Fig. S9. Elemental composition calculator of **3** $C_8H_{11}N_4O_2$. Calc. 195.087652, -0.892786 ppm error.

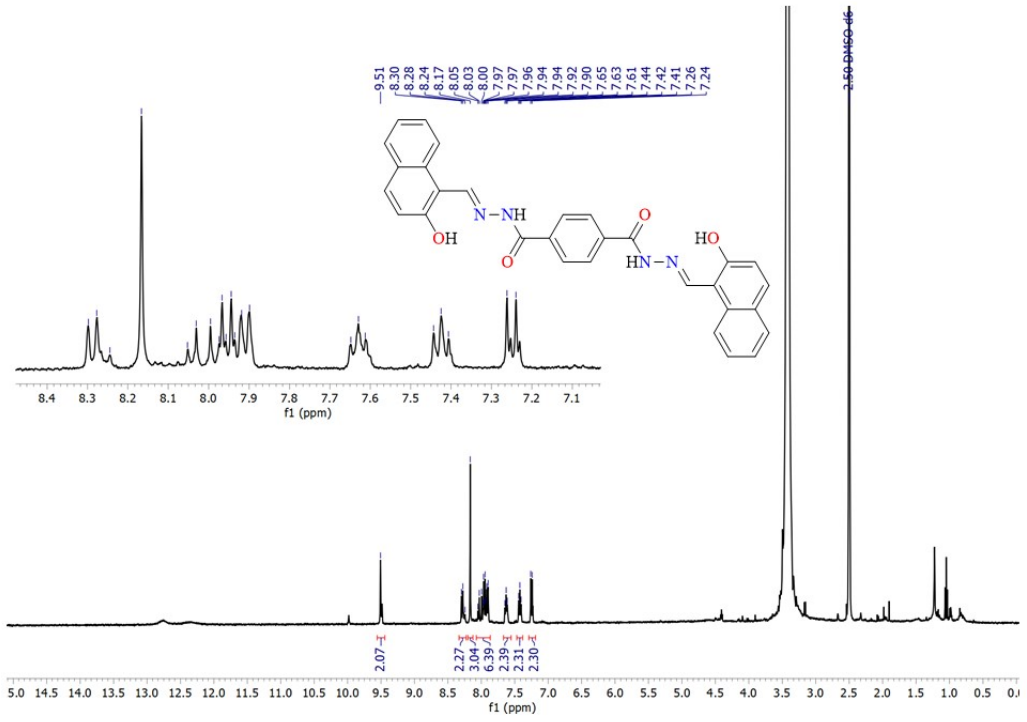

Fig. S10. ^{1}H NMR (400 MHz, $CDCl_3$) spectrum of ligand **4**.

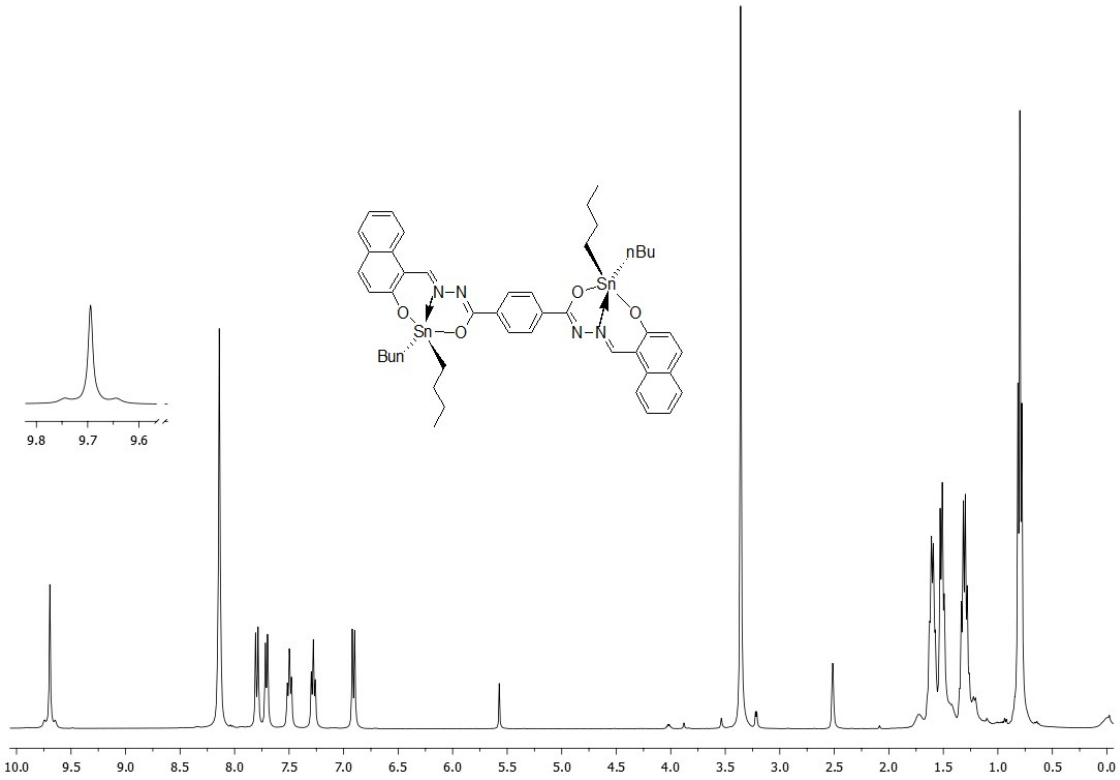

Fig. S11. ^{1}H NMR (400 MHz, $CDCl_3$) spectrum of compound **5**.

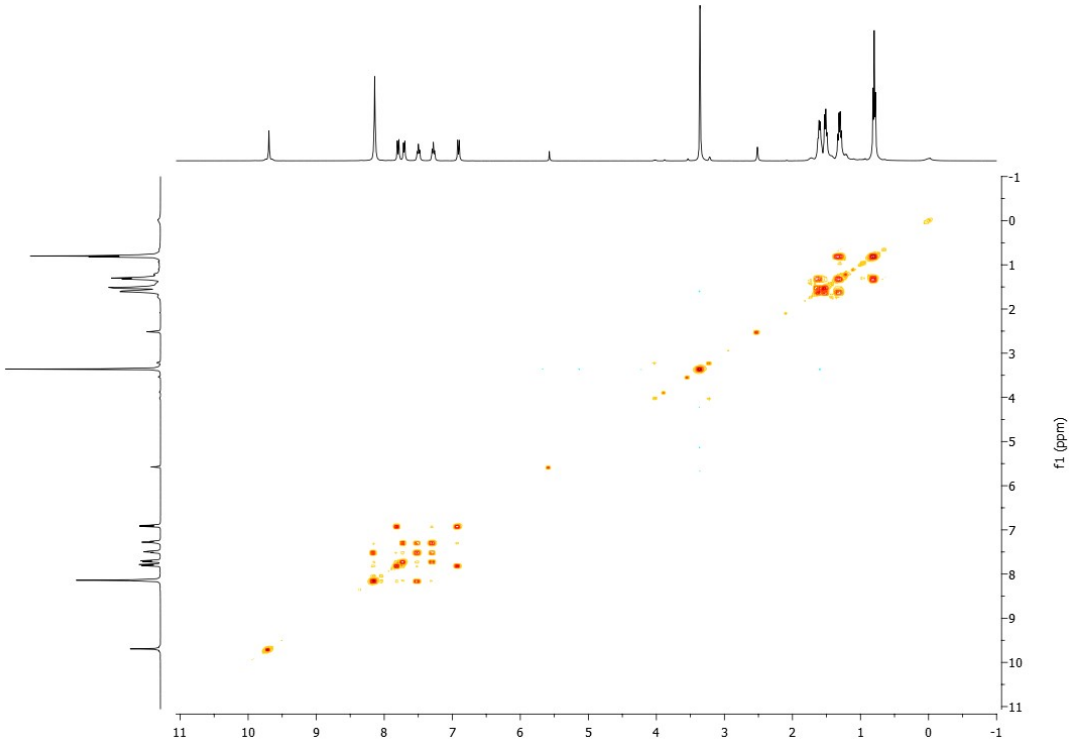

Fig. S12. COSY ($CDCl_3$) spectrum of organotin compound **5.**

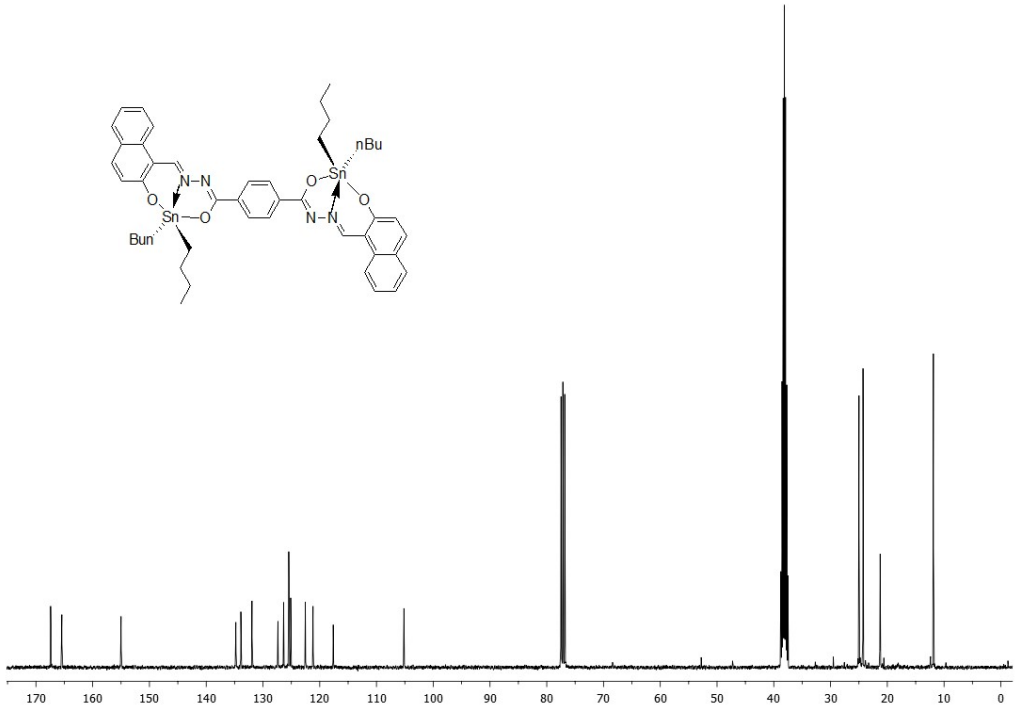

Fig. S13. ^{13}C NMR (100 MHz, $CDCl_3$) spectrum of compound **5**.

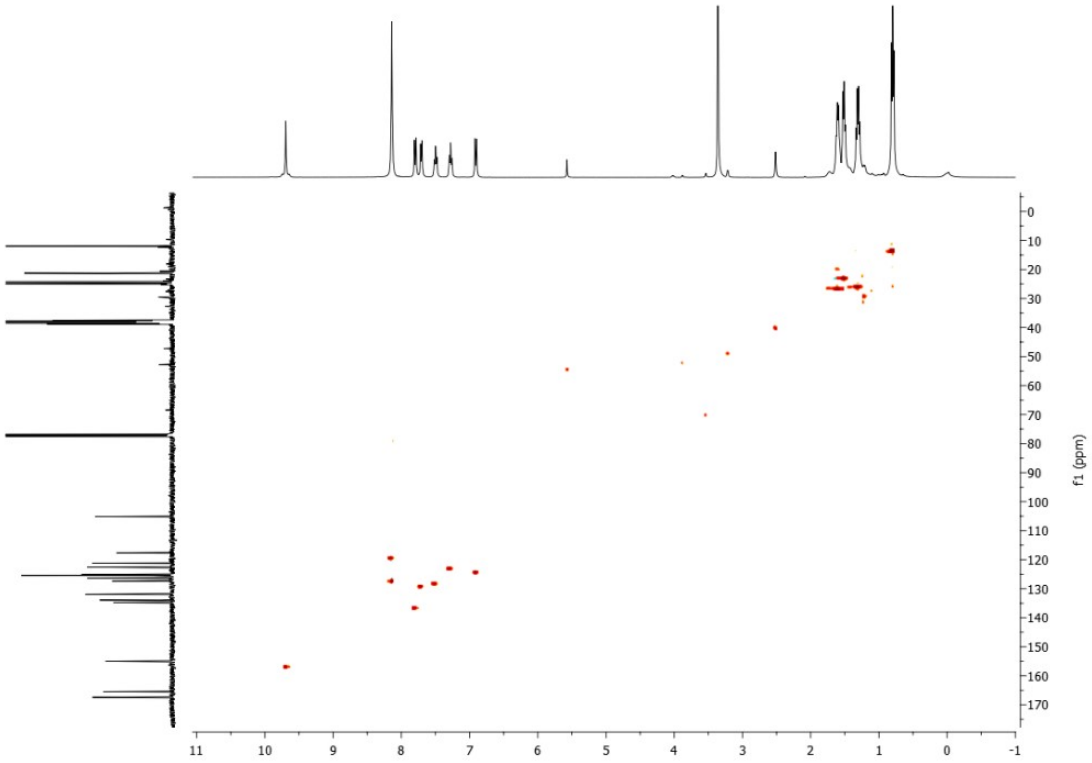

Fig. S14. HETCOR ($CDCl_3$) spectrum of organotin compound **5**.

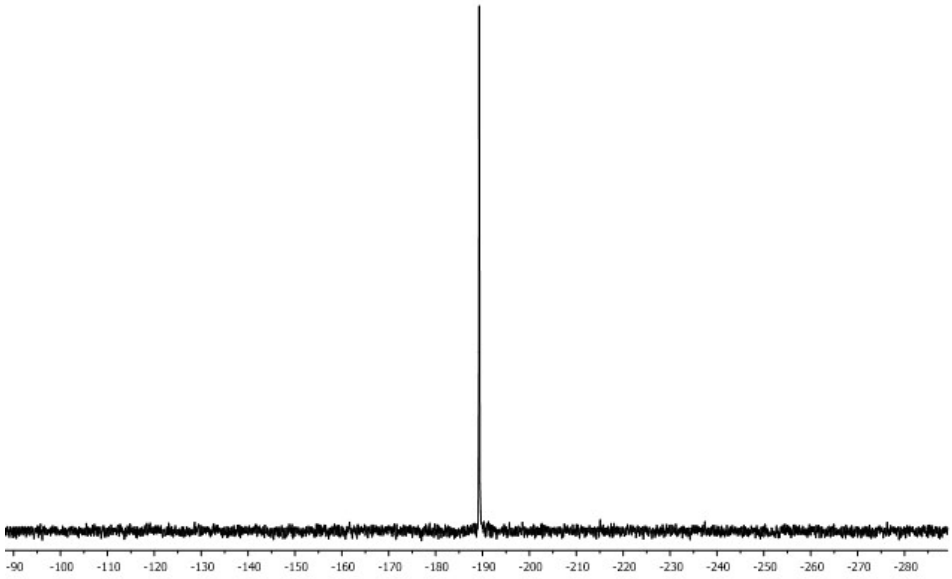

Fig. S15. ^{119}Sn NMR (149 MHz, $CDCl_3$) spectrum of compound **5**.

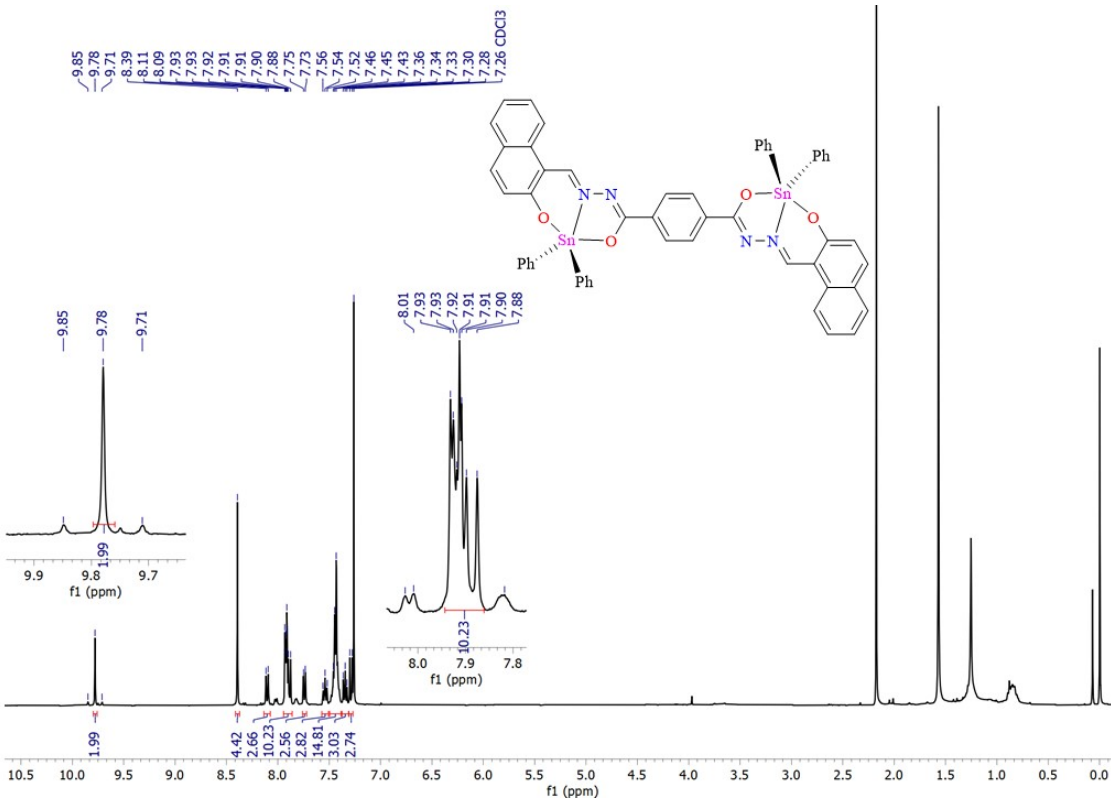

Fig. S16. ^{1}H NMR (400 MHz, $CDCl_3$) spectrum of compound **6**.

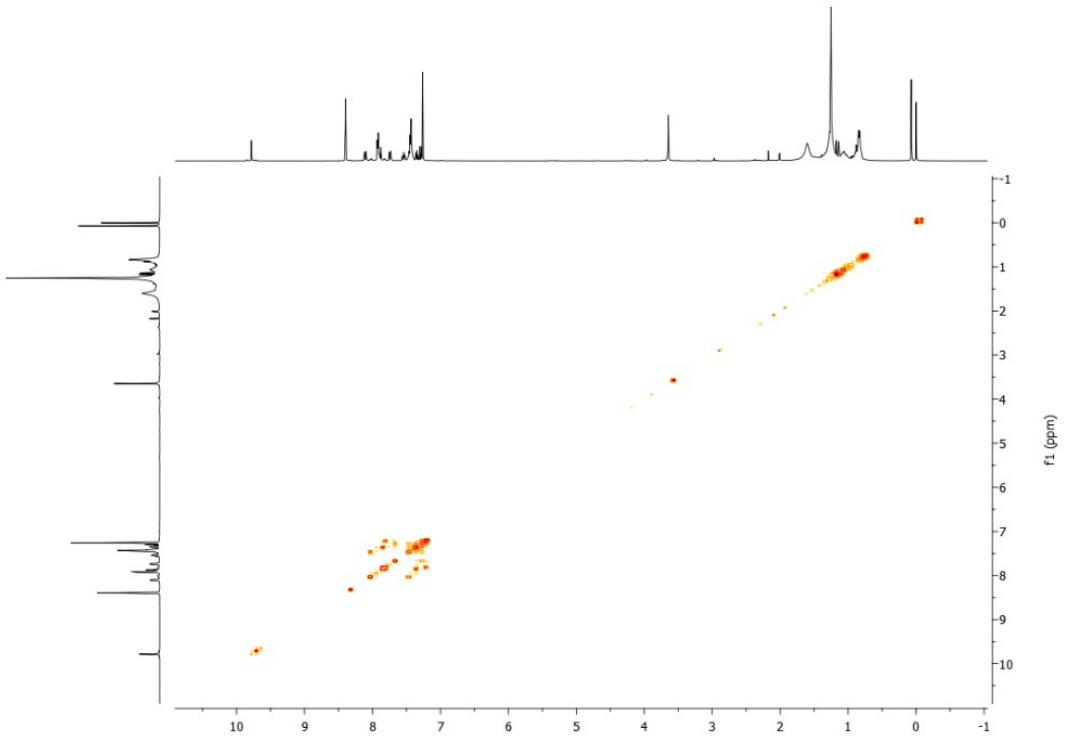

Fig. S17. COSY ($CDCl_3$) spectrum of organotin compound **6**.

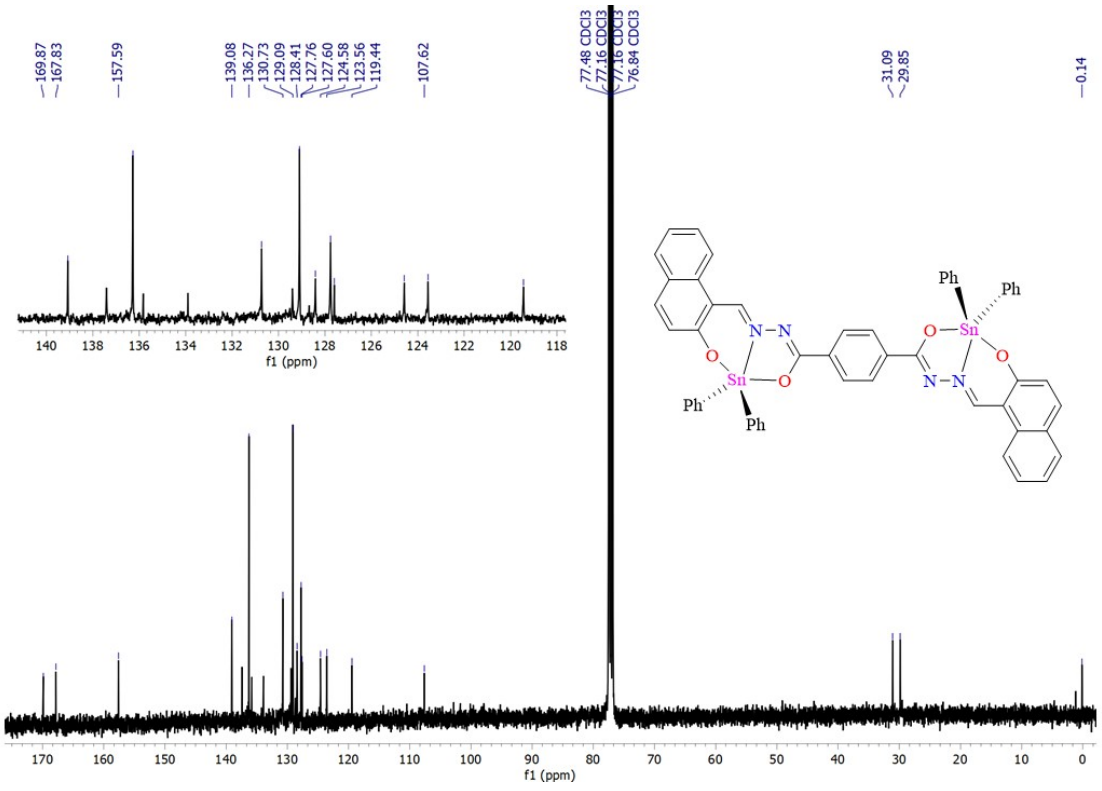

Fig. S18. ^{13}C NMR (100.16 MHz, $CDCl_3$) spectrum of compound **6.**

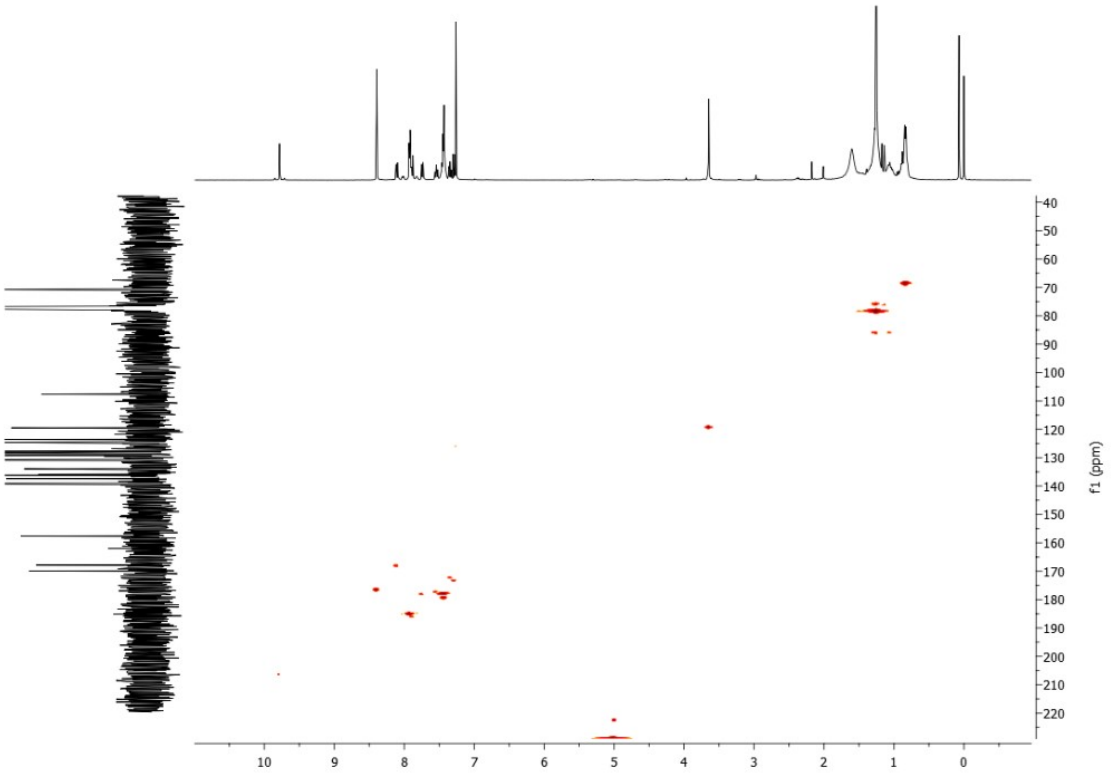

Fig. S19. HETCOR ($CDCl_3$) spectrum of organotin compound **6**.

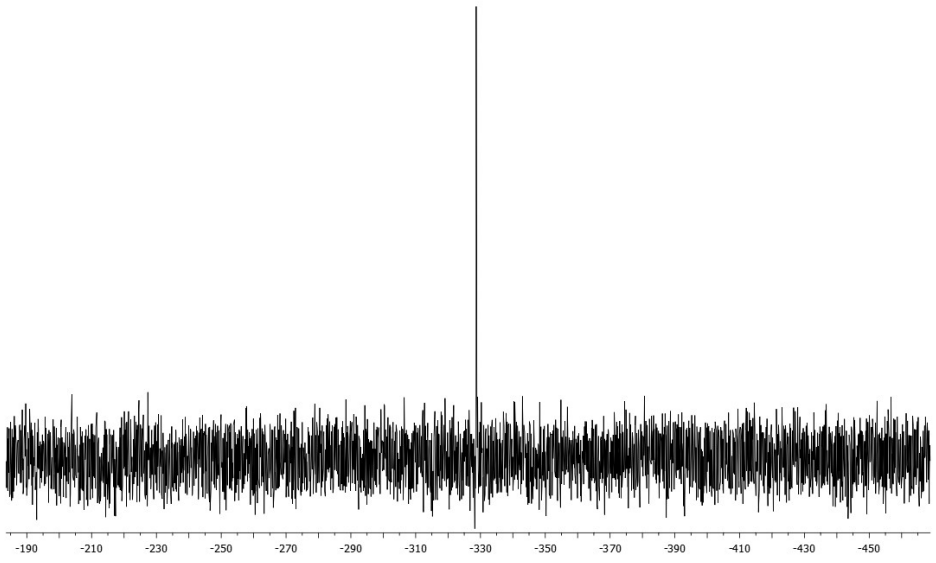

Fig. S20. ^{119}Sn NMR (149 MHz, $CDCl_3$) spectrum of compound **6.**

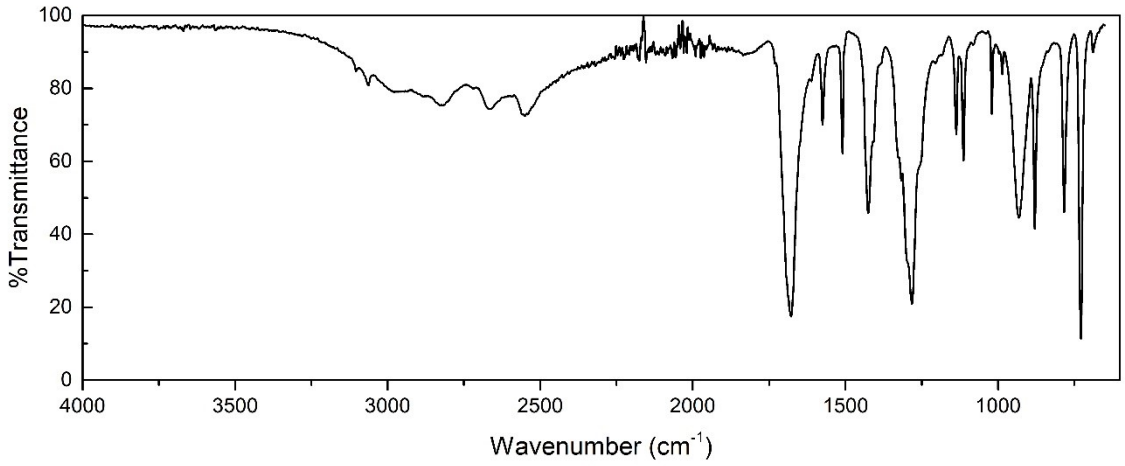

Fig. S21. Infrared spectrum of terephthalic acid obtained from PET waste.

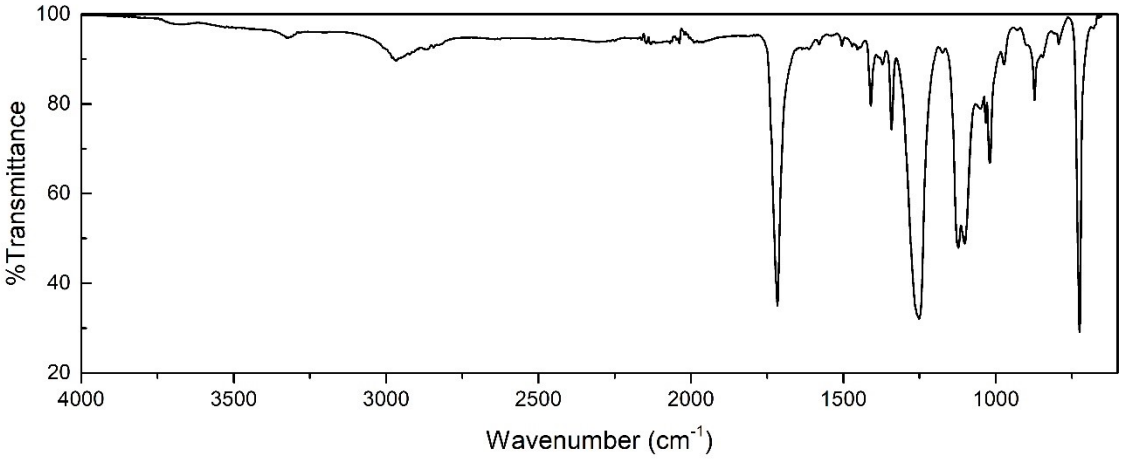

Fig. S22. Infrared spectrum of **1** obtained from PET waste.

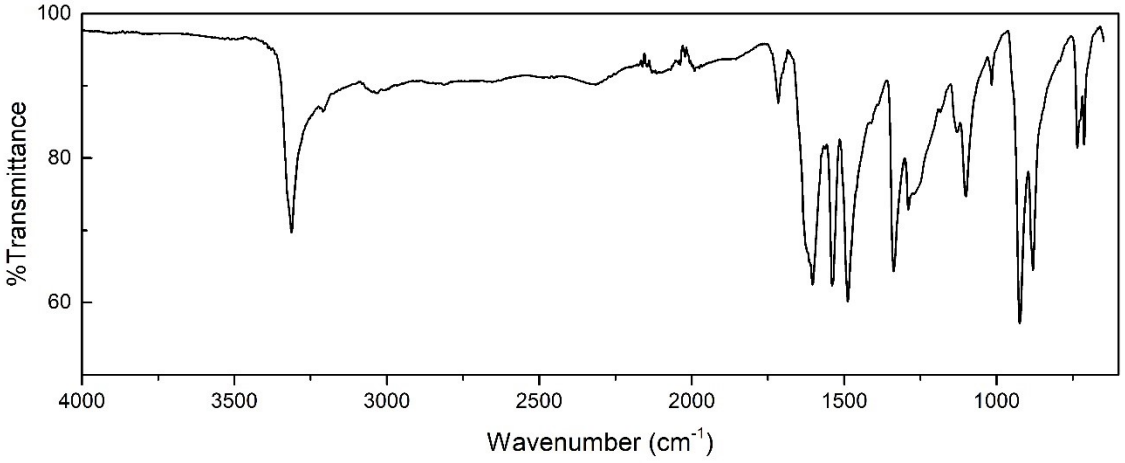

Fig. S23. Infrared spectrum of **3** obtained from PET waste.

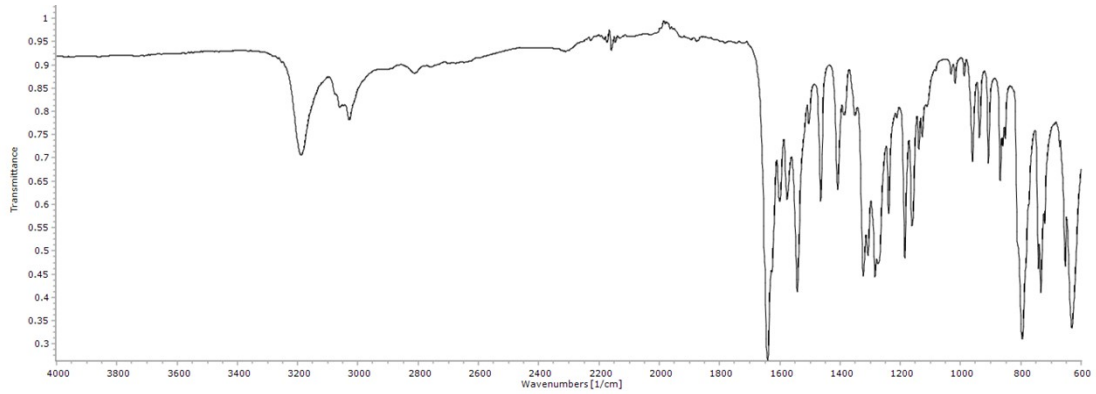

Fig. S24. Infrared spectrum of compound **4.**

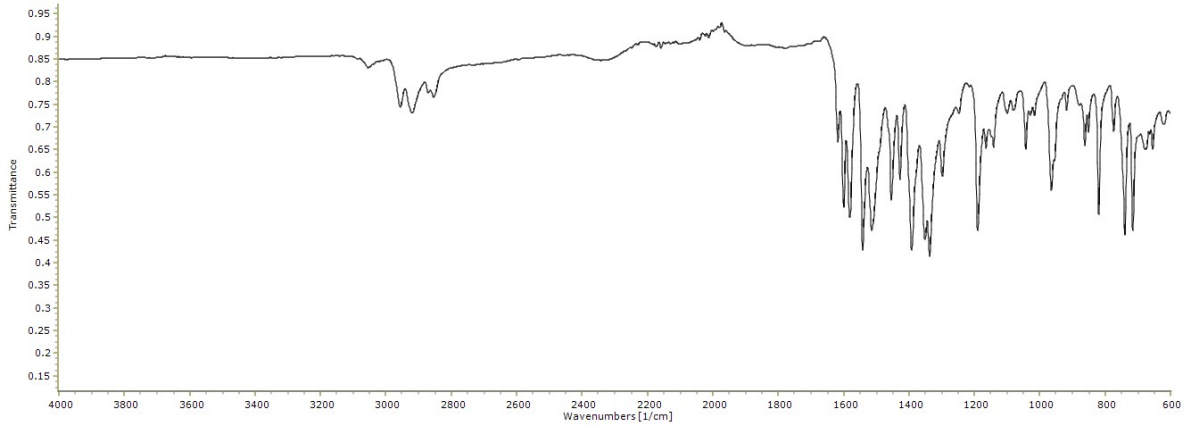

Fig. S25. Infrared spectrum of compound **5**.

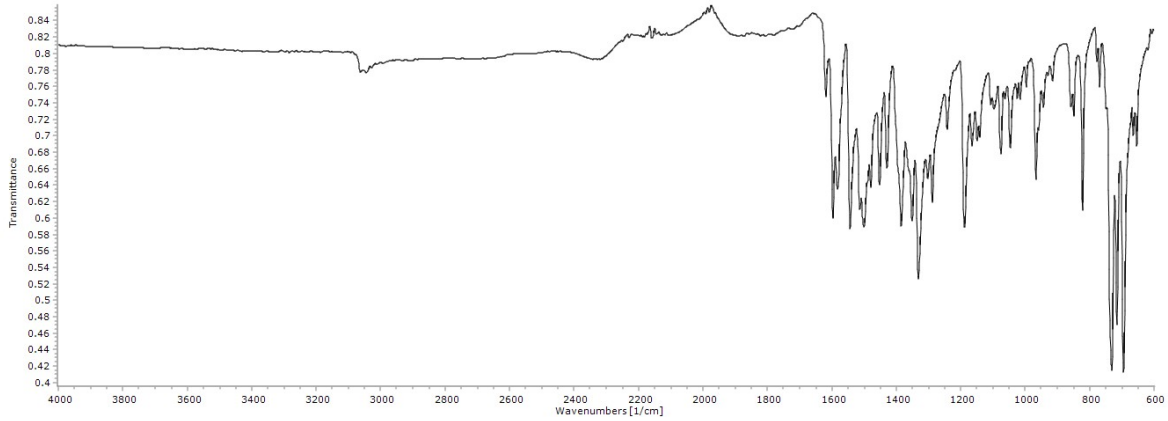

Fig. S26. Infrared spectrum of compound **6.**

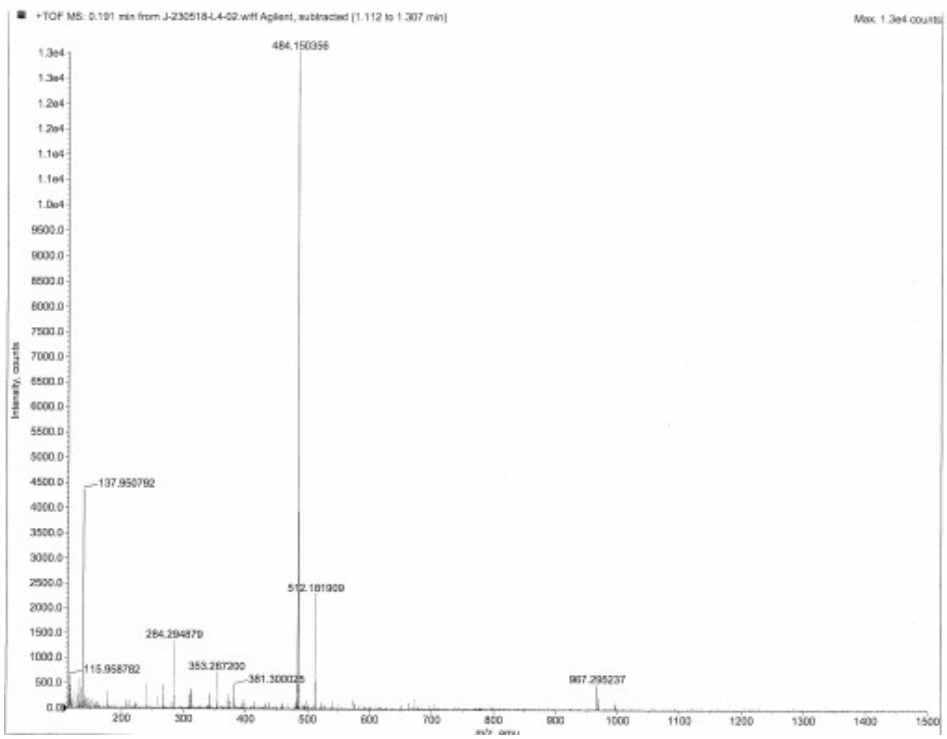

Fig. S27. High resolution mass spectrum of compound **4**.

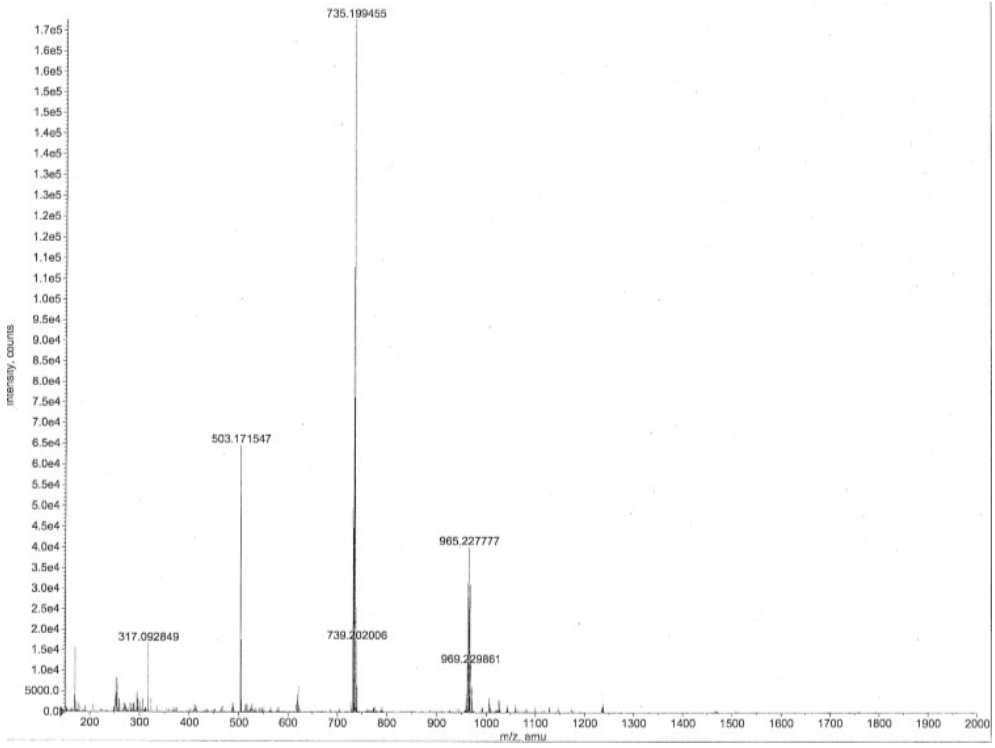

Fig. S28. High resolution mass spectrum of compound **5**.

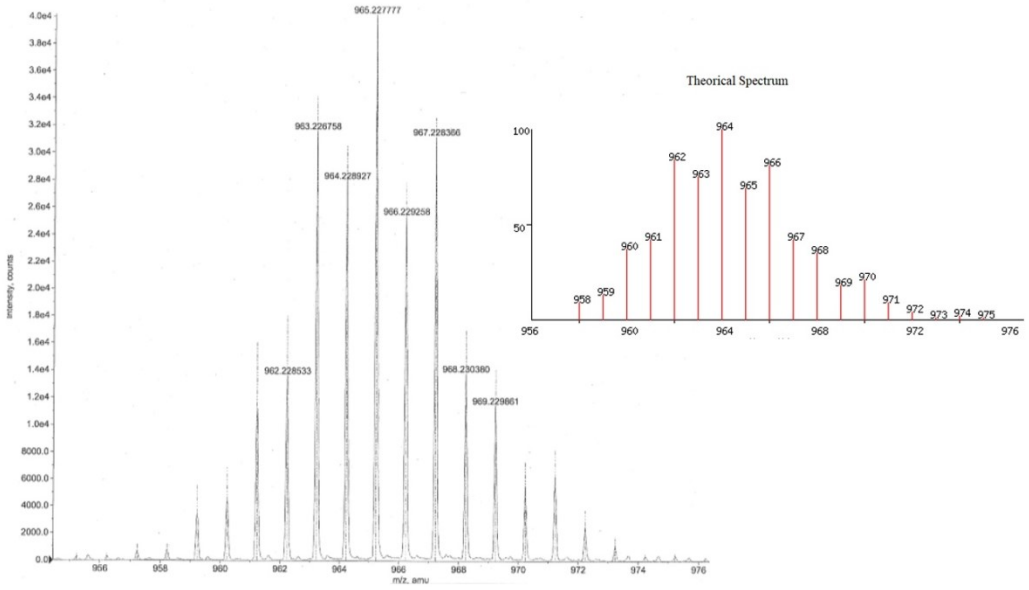

Fig. S29. Isotopic pattern of compound **5**.

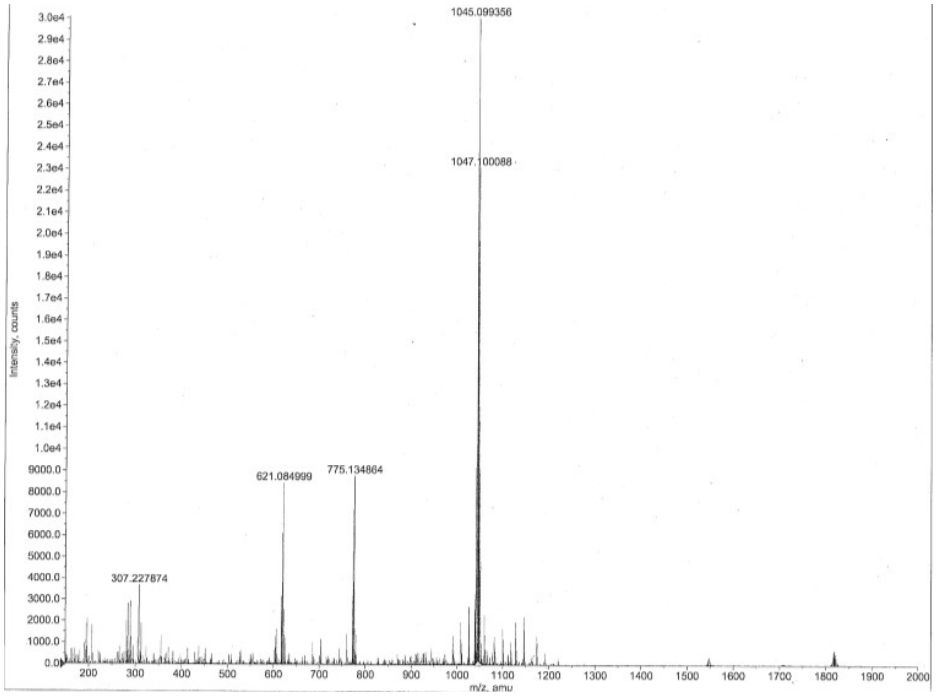

Fig. S30. High resolution mass spectrum of compound **6**.

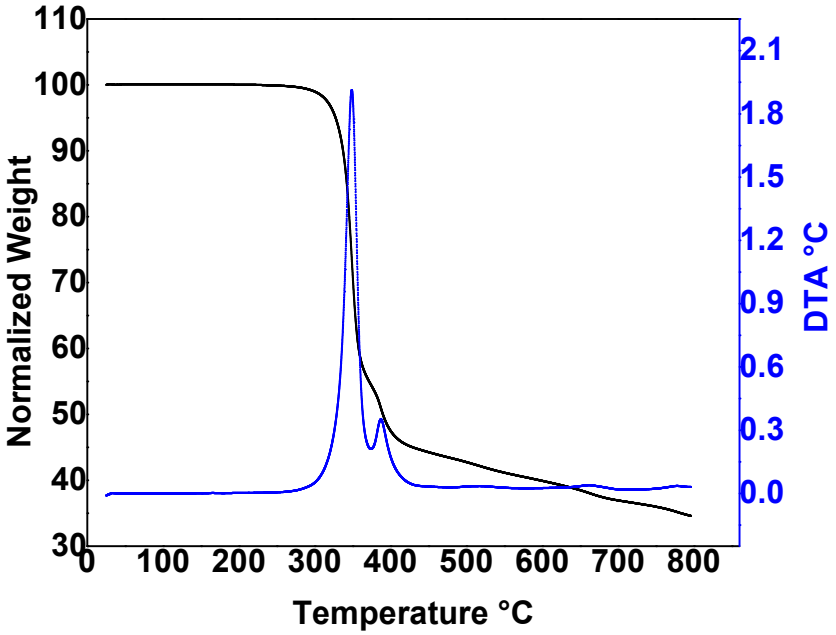

Fig. S31. Thermogravimetric Analysis of compound **5**.

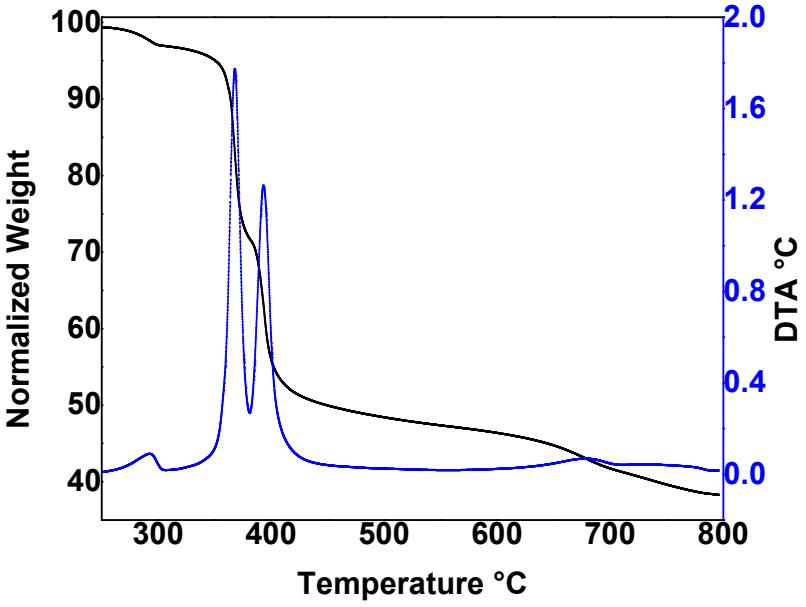

Fig. S32. Thermogravimetric Analysis of compound **6**.

Table S2. Calculated wavelength (λ) and oscillator strength (f, approximated to the first two digits) for the 30 excitations of complex **5** and **6.**

5

Excitation	λ(nm)	f
1	464.3	1.40
2	423.8	0.11
3	395.8	0.09
4	378.0	0.15
5	340.9	0.15
6	336.2	0.23
7	328.1	0.01
8	317.1	0.03
9	312.0	0.15
10	306.4	0.04
11	305.1	0.04
12	302.5	0.00
13	301.7	0.00
14	301.0	0.06
15	300.3	0.00
16	296.2	0.00
17	290.0	0.04
18	288.5	0.19
19	285.0	0.01
20	281.1	0.00
21	279.5	0.06
22	278.7	0.01
23	276.8	0.00
24	274.4	0.11
25	273.3	0.00
26	270.4	0.03
27	268.7	0.22
28	268.2	0.00
29	263.3	0.01
30	262.1	0.03

6

Excitation	λ(nm)	f
1	460.2	1.46
2	416.9	0.11
3	392.0	0.11
4	372.3	0.16
5	342.5	0.10
6	339.1	0.24
7	324.7	0.01
8	313.0	0.19
9	312.0	0.01
10	306.0	0.07
11	304.5	0.04
12	303.9	0.00
13	303.9	0.00
14	303.2	0.01
15	301.9	0.00
16	301.7	0.00
17	297.1	0.04
18	292.9	0.00
19	292.3	0.01
20	292.2	0.00
21	292.0	0.00
22	292.0	0.00
23	291.8	0.00
24	291.7	0.00
25	290.3	0.03
26	290.1	0.07
27	290.0	0.00
28	286.3	0.00
29	280.3	0.00
30	277.0	0.00

Table S3. Fluorescence lifetimes in chloroform at different excitation and fluorescence emission value

Compound	Laser (nm)	λ_{em} (nm)	τ (ns)	χ^2
5	370	496	1.80	1.18
		533	1.82	1.20
		571	1.83	1.10
	455	496	1.76	1.16
		533	1.77	1.08
		571	1.78	1.06
6	370	492	2.14	1.05
		527	2.17	1.16
		569	2.18	1.22
	455	492	2.02	1.18
		527	2.03	1.00
		569	2.05	1.20

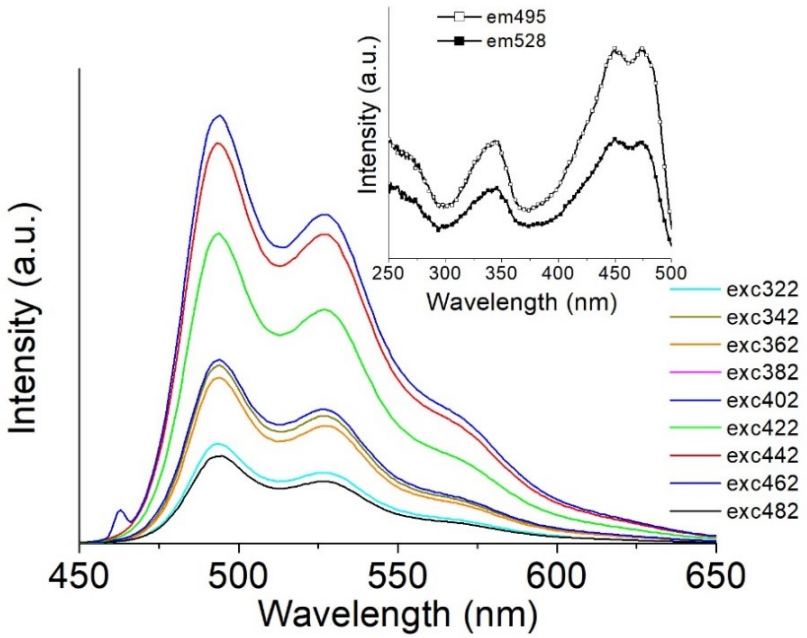

Fig. S33. Fluorescence spectra of organotin compound **5** in $CHCl_3$ at different excitation wavelength. Inserted figure: corresponding excitation spectrum by fixing as emission value, the peak at 495 nm or the shoulder at 528 nm.

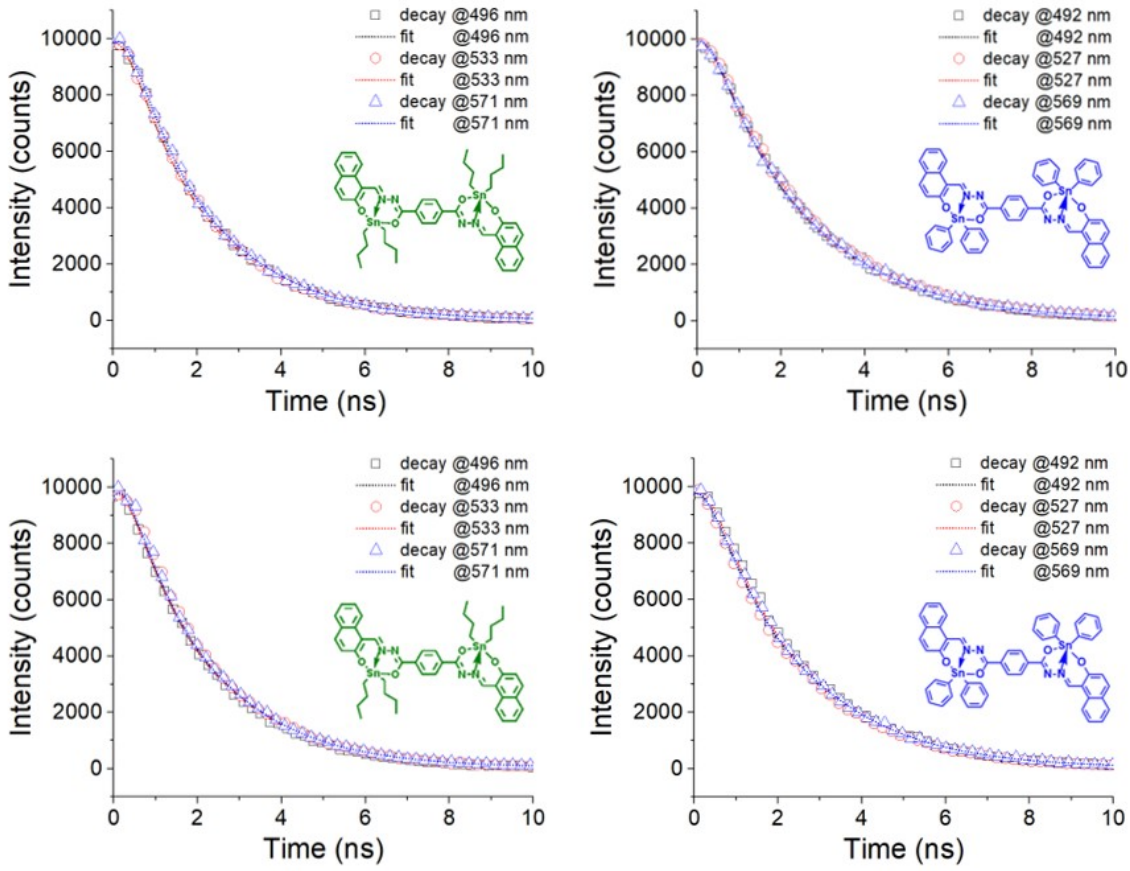

Fig. S34. TCSPC Fluorescence decay (symbols) and fit (dotted lines) of organotin compound **5** (left graphs) and **6** (right graphs) in $CHCl_3$ at 370 nm (top panel) or 455 nm (bottom panel) excitation. The emission wavelengths are specified in the legend.

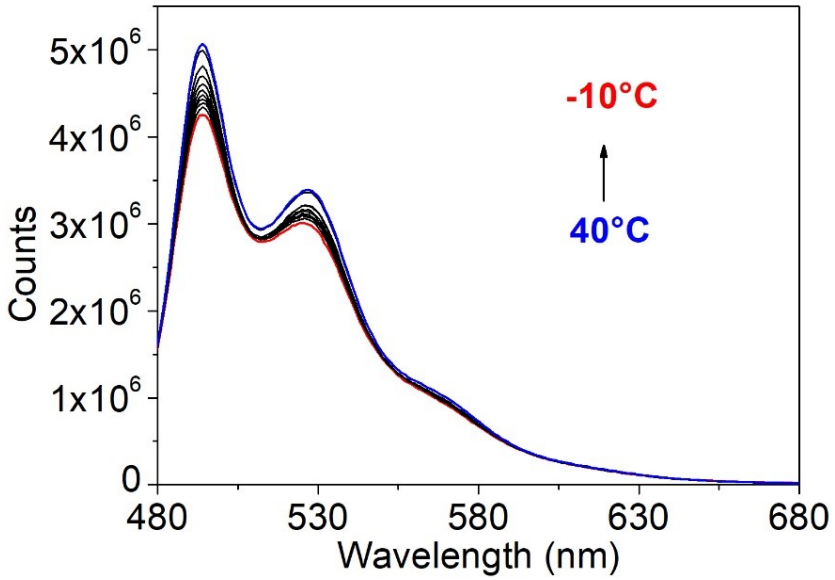

Fig. S35. Fluorescence spectra of organotin compound **6** in chloroform at different temperatures.

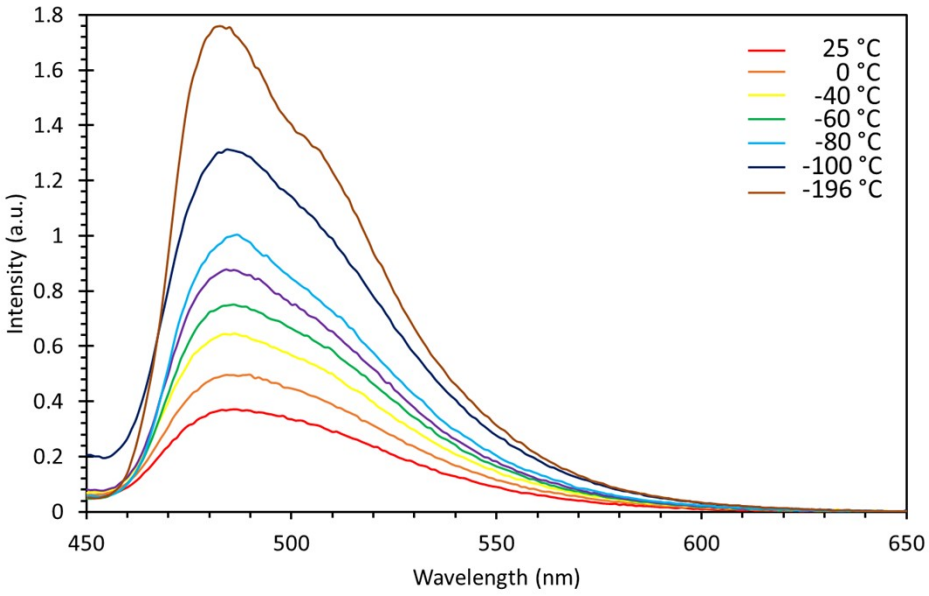

Fig. S36. Fluorescence spectra of ligand **4** in 2-methyl tetrahydrofuran ($5 \cdot 10^{-5}$ M) at different temperatures.

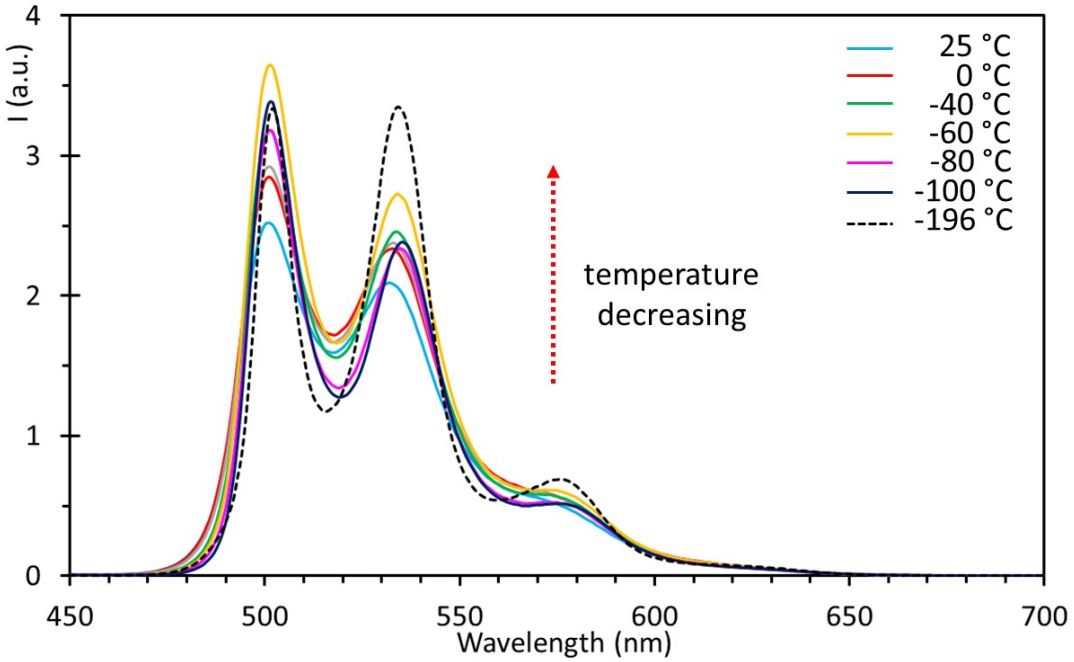

Fig. S37. Fluorescence spectra of organotin compound **5** in 2-methyl tetrahydrofuran ($5 \cdot 10^{-5}$ M) at different temperatures.

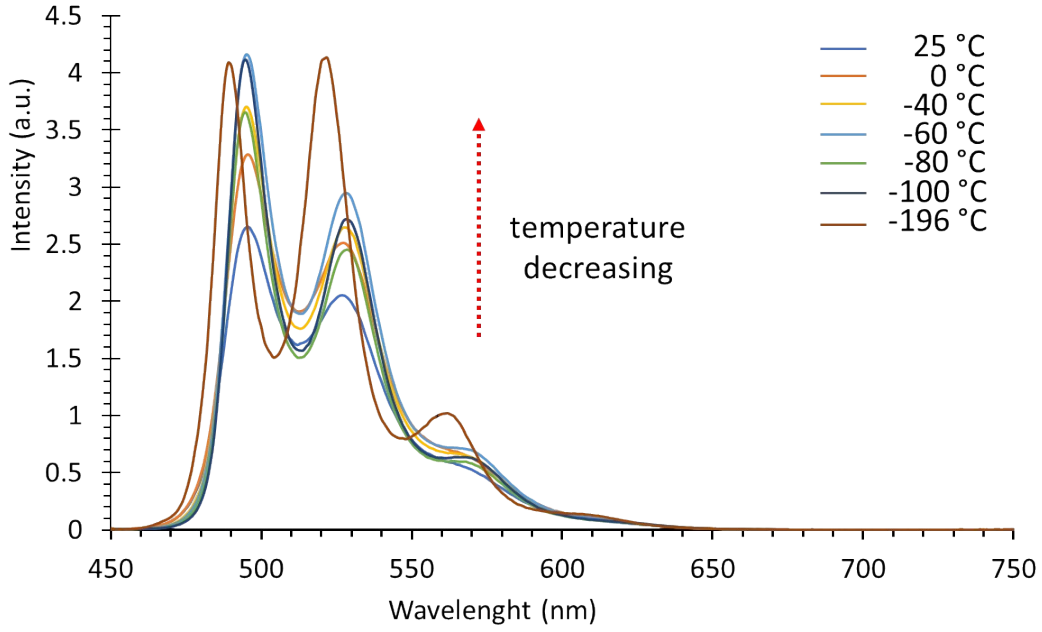

Fig. S38. Fluorescence spectra of organotin compound **6** in 2-methyl tetrahydrofuran ($5 \cdot 10^{-5}$ M) at different temperatures.

Table S4. Average weighted fluorescence lifetimes of complex **5**, at different temperatures, recorded in 2-methyl tetrahydrofuran ($5 \cdot 10^{-5}$ M).

T (°C)	average τ (ns) at 502 nm	average τ (ns) at 534 nm	average τ (ns) at 577 nm	Δ(502/534)	Δ(502/577)	Δ(534/577)
5	2.34	2.34	2.40	0.00	-0.06	-0.06
0	2.50	2.51	2.50	-0.01	0.00	0.01
-10	2.42	2.45	2.52	-0.02	-0.09	-0.07
-40	2.56	2.58	2.62	-0.02	-0.06	-0.04
-60	2.72	2.78	2.74	-0.06	-0.02	0.04
-80	2.77	2.84	2.88	-0.07	-0.11	-0.05
-100	2.84	2.86	2.87	-0.02	-0.03	-0.01
-196	2.70	2.72	2.73	-0.02	-0.02	0.00

Table S5. Fluorescence lifetimes of compound **4**, at different temperatures, recorded in 2-methyl tetrahydrofuran ($5 \cdot 10^{-5}$ M).

T (°C)	τ at 488 nm (ns)	Goodness of fit (χ^2)	average τ (ns) at 488 nm	τ at 509 nm (ns)	Goodness of fit (χ^2)	average τ (ns) at 509 nm
5	0.74 (91.04%) 3.36 (8.96%)	1.007	0.97	0.78 (93.60%) 3.60 (6.40%)	1.003	0.96
0	0.75 (82.71%) 2.15 (17.29%)	1.098	0.99	0.82 (91.39%) 2.85 (8.61%)	1.019	0.99
-10	0.97 (87.44%) 2.75 (12.56%)	1.119	1.19	0.91 (64.89) 3.20 (35.11%)	1.017	1.71
-40	1.05 (80.99%) 2.43 (19.01%)	0.894	1.31	1.19 (93.41%) 3.20 (6.59%)	1.100	1.32
-60	1.20 (86.20%) 2.98 (13.80%)	1.027	1.45	1.26 (91.25%) 3.53 (8.75%)	0.912	1.46
-80	1.19 (70.02%) 2.42 (29.98%)	1.152	1.56	1.09 (66.36%) 2.29 (33.64%)	0.980	1.49
-100	1.40 (87.67%) 3.32 (12.33%)	1.058	1.64	1.32 (82.16%) 2.79 (17.84%)	1.087	1.58
-196	1.51 (65.68%) 3.00 (34.32%)	1.000	2.02	1.37 (57.08%) 2.71 (42.92%)	1.125	1.95

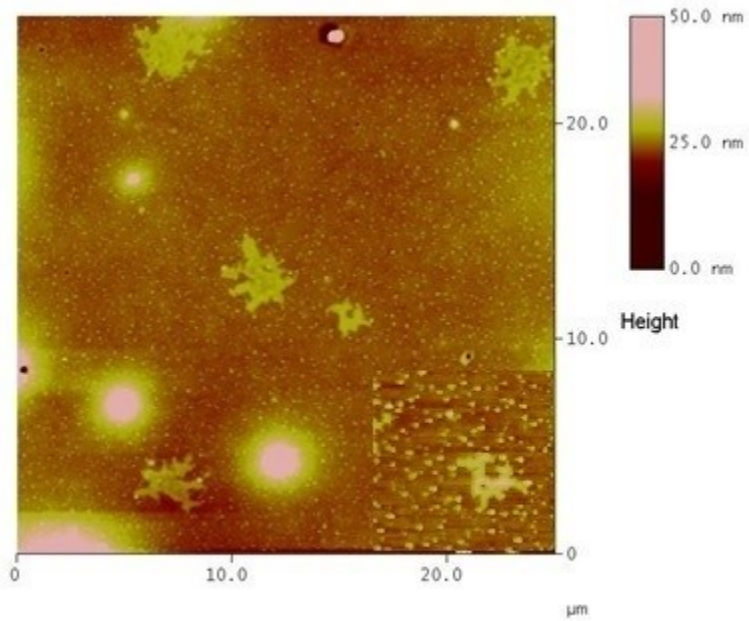

Fig. S39. Tapping AFM image of thin film prepared from chlorobenzene solutions of complex **5** in 25 µm*25 µm scanning area and (inset) 5 µm*5µm.

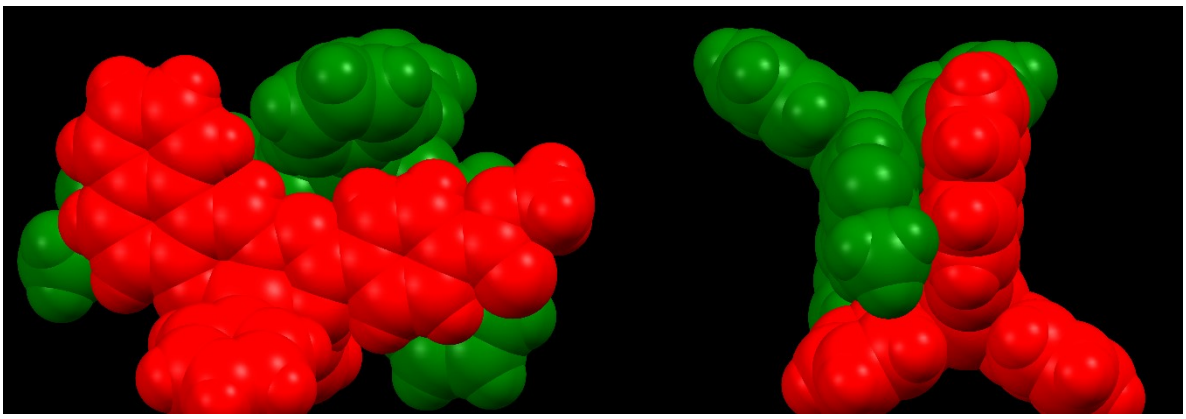

Fig. S40. Molecular structure of compound **8**.

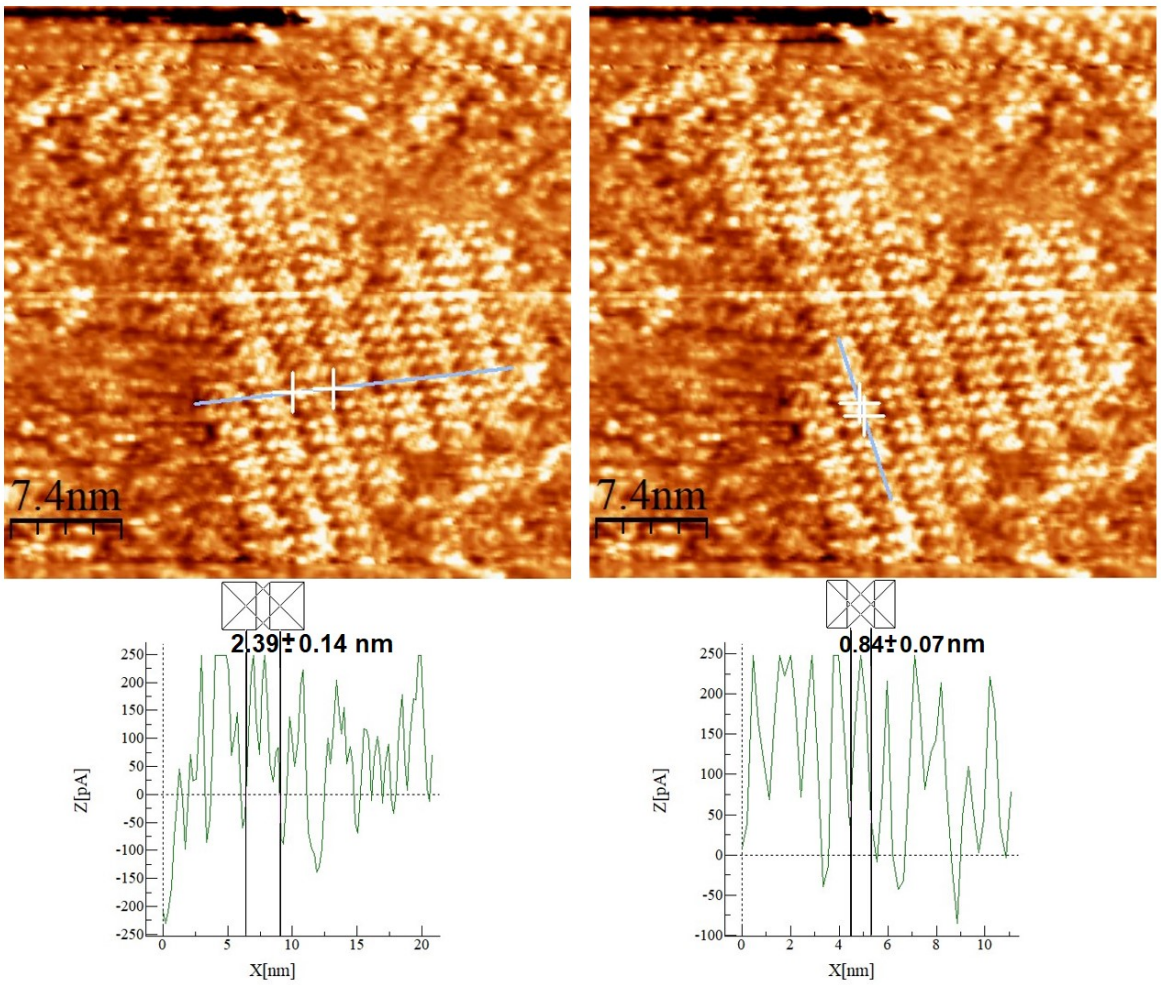

Fig. S41. Current profiles of Sn-complex **5** at different orientations as signaled in the STM image: for the lamellae length determination and right) for the individual molecules length determination: Vbias = -740 mV, It = 90 pA.

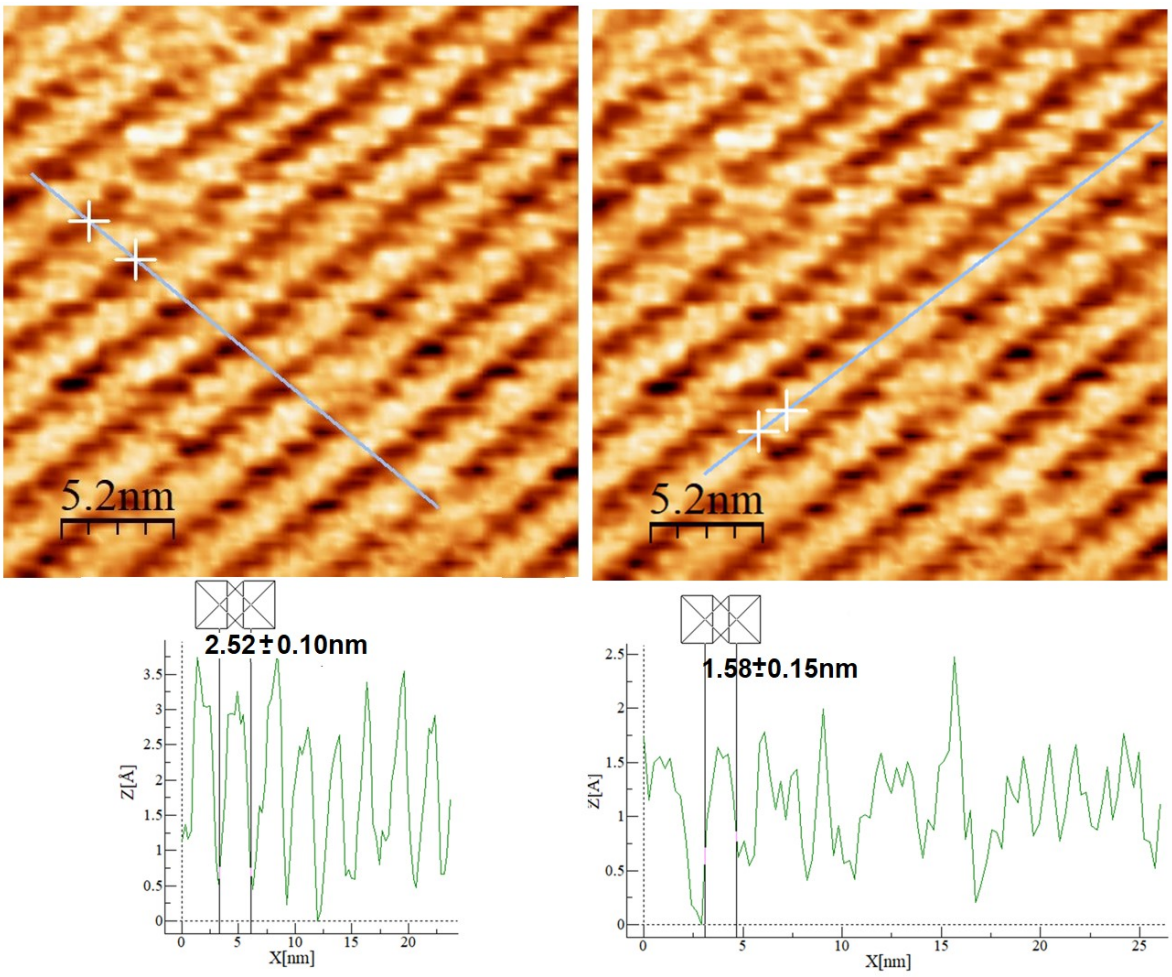

Fig. S42. Topographic profiles of Sn-complex **6** at different orientations as signaled in the STM image: left) for the lamellae length determination and right) for the individual molecule's length determination: Vbias = -830 mV, It = 110 pA.

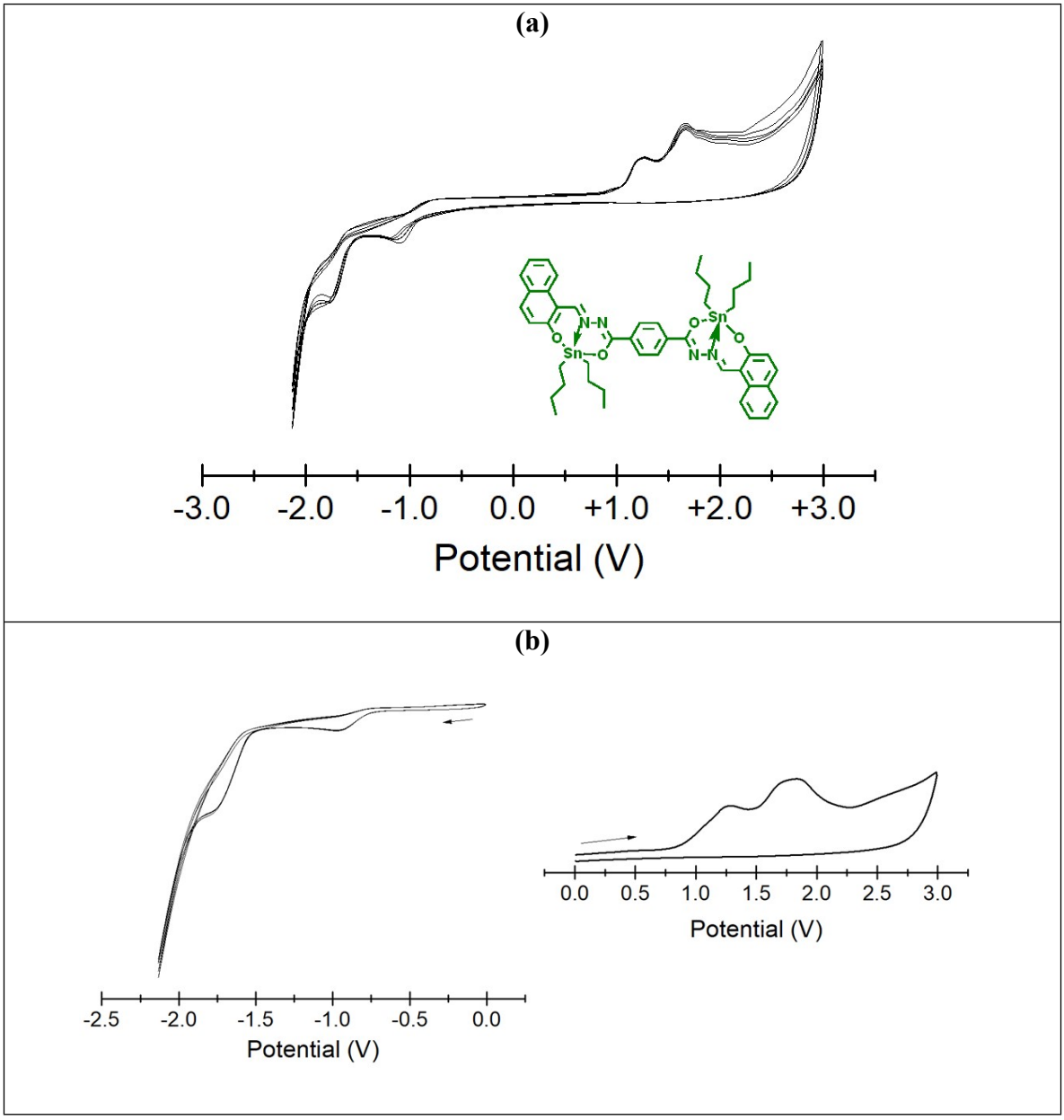

Fig. S43. (a) Successive cyclic voltammogram of binuclear Sn-complex **5** in CH_2Cl_2 (0.1 mmol), at scan rate of 50mV/s vs. Ag/AgCl, using GC as working electrode and 0.1 M Bu_4NPF_6 as supporting electrolyte. (b) Cyclic voltammograms of the (left) reductive (0 to +3 V) and (right) oxidative (0 to -2.40 V). By analysing the redox process by separate, this is not achieved completely (as occurs with the complete cycle), because in order to reduce **5**, it first needs to be oxidized and *vice versa.* However, some signals are observed, because anions or cations can individually be stabilized within the structure.

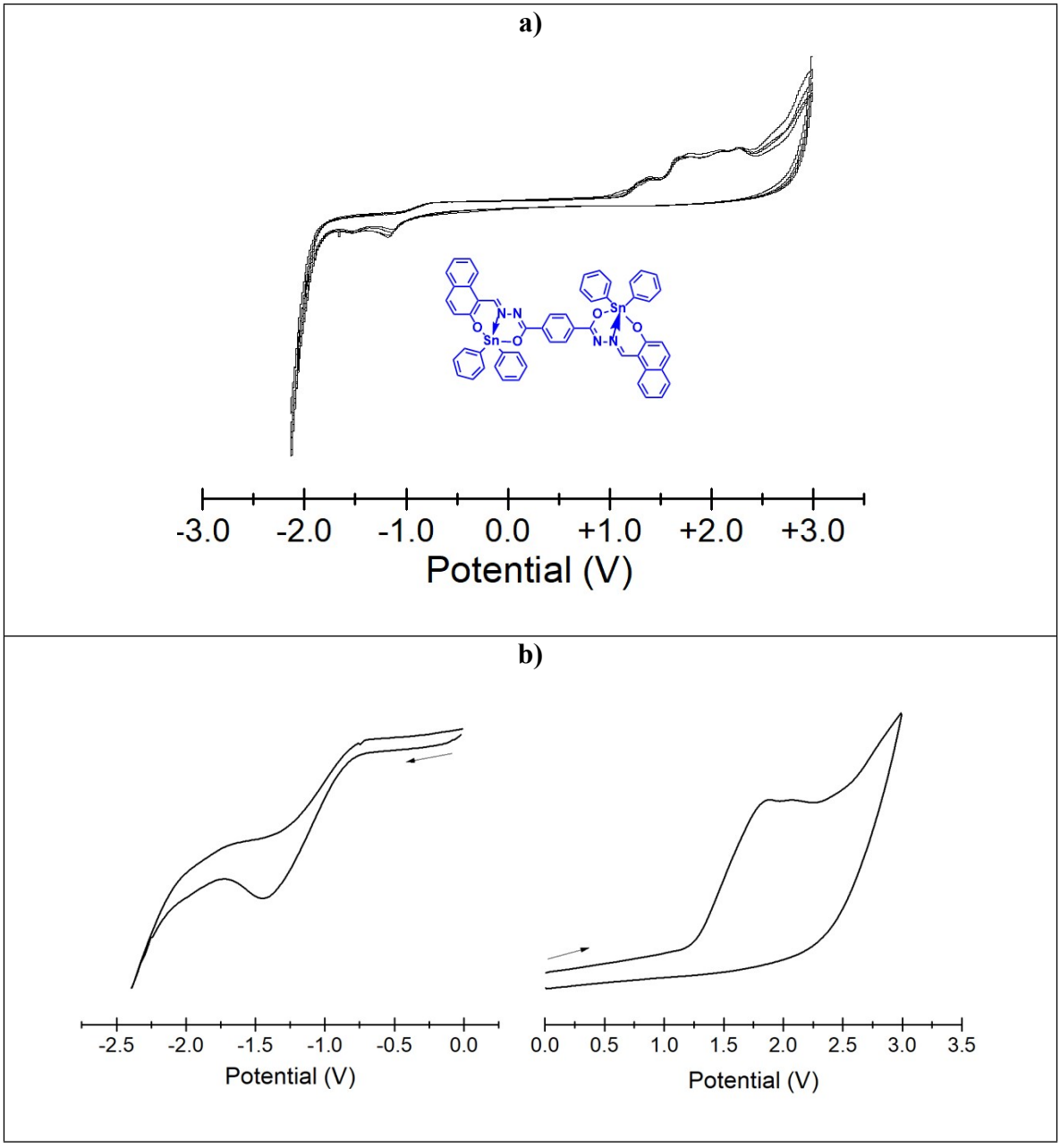

Fig. S44. (a) Successive cyclic voltammogram of binuclear Sn-complex **6** in CH_2Cl_2 (0.1 mmol), at scan rate of 50mV/s vs. Ag/AgCl, using GC as working electrode and 0.1 M Bu_4NPF_6 as supporting electrolyte. (b) Cyclic voltammograms of the (left) reductive (0 to +3 V) and (right) oxidative (0 to -2.40 V). By analysing the redox process by separate, this is not achieved completely (as occurs with the complete cycle), because in order to reduce **6**, it first needs to be oxidized and *vice versa.* However, some signals are observed, because anions or cations can individually be stabilized within the structure.

References

[1] F. Neese, F. Wennmohs, U. Becker, C. Riplinger, *J. Chem. Phys.,* 2020, **152**, 224108.

[2] R. Cammi, B. Mennucci, J. Tomasi, *J. Phys. Chem. A,* **2000**, **104**, 5631.

[3] a) S. Grimmea, J. Antony, S. Ehrlich, H. Krieg, *J. Chem. Phys*. 2010, **132**, 154104. b) S. Grimme, S. Ehrlich, L. Goerigk, L. *J. Comput. Chem*. 2011, **32**, 1456-1465.

[4] a) E. van Lenthe, E. J. Baerends, J. G. Snijders, *J. Chem. Phys.* 1993, **99**, 4597 (1993) b) E. van Lenthe, E. J. Baerends, J. G. Snijders, *J. Chem. Phys.* 1994, **101**, 9783. c) C. van Wüllenhttps, *J. Chem. Phys.* 1998, **109**, 392.

[5] F. Weigenda, R. Ahlrich, *Phys. Chem. Chem. Phys.* 2005, **7**, 3297-3305.

[6] J. D. Rolfes, F. Neese, D. A. Pantazis, *J. Comput. Chem.* 2020, **41**, 1842-1849.

[7] T. Lu and F. Chen, *J. Comput. Chem.* 2012, **33**, 580-592.

[8] W. Humphrey, A. Dalke, and K. Schulten, *J. Mol. Graph.* 1996, **14**, 33-38.

[9] A. Felouat, A. D'Aléo, F. Fages, *J. Org. Chem.* 2013, **78**, 4446–4455.

[10] G. M. Sheldrick, *Acta Crystallogr. Sect. A*. 1990, **46**, 467–473.

[11] G. M. Sheldrick, SHELX-97: Program for the solution and refinement of crystal structures; Universität Göttingen: Göttingen, Germany, **1997**.

[12] L. J. Farrugia, *J. Appl. Crystallogr.* 1999, **32**, 837–838.

[13] I. Horcas, R. Fernández, J. M. Gómez-Rodríguez, J. Colchero, J. Gómez-Herrero, A. M. Baro, *Rev. Scien. Instrum.*, 2007, **78**, 013705.

[14] H. Hosseini-Monfared, N. Asghari-Lalami, A. Pazio, K. Wozniak, C. Janiak, *Inorg. Chim. Acta.* 2013, **406**, 241–250.

[15] a) B. K. Lakshmi, N. Shivananda, G. A. Prakash, A. M. Isloor, K. N. Mahendra, *Bull. Korean Chem. Soc*. 2012, **33**, 673–482. b) P. G. Avaji, C. H. Vinod, A. Sangamesh, K. N. Shivananda, C. Bagaraju, *Eur. J. Med. Chem*. 2009, **44**, 3552–3559.

[16] X. Zhang, B. Tang, P. Zhang, M. Li, M. Jing, W. Tian, *J. Mol. Struct.* 2007, **846**, 55–64.